universität wien

MASTERARBEIT / MASTER'S THESIS

Titel der Masterarbeit / Title of the Master's Thesis

„Reconstruction of Projection Orientations in Cryo-Electron Microscopy“

verfasst von / submitted by

Denise Schmutz, BSc

angestrebter akademischer Grad / in partial fulfilment of the requirements for the degree of

Master of Science (MSc)

Wien, 2017 / Vienna, 2017

Studienkennzahl lt. Studienblatt / degree programme code as it appears on the student record sheet:	A 066 821
Studienrichtung lt. Studienblatt / degree programme as it appears on the student record sheet:	Masterstudium Mathematik UG2002
Betreut von / Supervisor:	Univ.-Prof. Dipl.-Ing. Dr. Otmar Scherzer

Contents

I.Introduction

An inverse problem is a problem where the result is known and the cause should be calculated. A typical area where such questions appear is medical imaging, for example in computer tomography, where X-ray beams are sent through some part of the body in order to generate a series of two-dimensional images at certain angles. The inverse problem then consists of reconstructing the radiated body part given these images, that is calculating the density function describing the object. When particles are imaged in cryo-electron microscopy the situation is very similar, but due to the nature of the experiment, aside from the object itself also the directions in which the electron beams pass through the object are unknown. This thesis is concerned with different methods to solve the inverse problem of recovering the relative orientations of images taken in cryo-electron microscopy and different methods.

1. Cryo-Electron Microscopy

In cryo-electron microscopy a sample consisting of a large number of identical particles is imaged at cryogenic conditions using a transmission electron microscope [Mil+13]. Put simply, in transmission electron microscopy a thin specimen is irradiated with an electron beam, similar to light microscopy, where visible photons are sent through the objects. The main difference is that due to the smaller wave length, the resolution that can be obtained in transmission electron microscopy is significantly higher. The interaction of the electrons with organic matter causes severe damage to the particles, so the electron dose needs to be low enough to preserve the structure of the specimen. That is the reason why the images obtained in cryo-EM are particularly noisy.

1.1. Single Particle Cryo-Electron Micrscopy

The specimen irradiated in cryo-EM consists of particles that are frozen and subsequently embedded in a thin layer of vitreous ice, preserving their native structure. As a result of this technique they lie in this layer of ice at random orientations. In this thesis we will focus on single particle cryo-EM (SPEM) in contrast to cryo-electron tomography (CET). While in CET the specimen is tilted and a series of projections is taken, in SPEM the non-tilted sample is only imaged once or very few times. This leads to data that contains the same information that would be obtained by taking projections of one single particle from random directions. The presentation of methods for

the reconstruction of these directions is the main goal of this thesis. For introductions to SPEM and cryo-EM in general see [Mil+13; Che15; Zho08; Sch+97].

2. Outline

In chapter II we begin with the definition of integral transforms and related spaces fundamental to this topic. Moreover, we fix the notion of a projection orientation and formulate the inverse problem appearing in cryo-EM in mathematical terms.
After having set the basics, we begin with discussing the *method of common lines* in chapter III. The calculation of the Euler angles defining the projection orientations builds the main part, followed by a section on the methods for line detection and an overview of further steps done in practice. Moreover, *model matching* is explained shortly as in a lot of cases it is combined with the common lines method. Considering the complexity of some ideas and the geometric aspects of the technique, we will not give any theorems and proofs in a strict sense.
In chapter IV we approach the *moment method*, which is barely used in practice as opposed to common lines, but still of theoretical interest. We also emphasize connections to chapter III with a special interest in uniqueness considerations.

II. Preliminaries

3. Basic transforms

Before we can formulate the problem of Cryo-EM in mathematical terms, we have to define some basic function spaces and transformations to work with. Most of the notation is adopted from [Nat01].
In the method of common lines the Fourier transform will play a crucial role as in the Fourier space the data possesses a certain geometric structure making it possible to recover the unknown directional information.

Definition 3.1. *The* Fourier transform *of $f \in L^1(\mathbb{R}^n)$ is defined as follows*

$$\mathcal{F}f(\boldsymbol{\eta}) = (2\pi)^{-n/2} \int_{\mathbb{R}^n} e^{i\boldsymbol{x}.\boldsymbol{\eta}} f(\boldsymbol{x}) d\boldsymbol{x}. \tag{3.1}$$

The inverse Fourier transform *is then given by*

$$\mathcal{F}^{-1}f(\boldsymbol{\eta}) = (2\pi)^{-n/2} \int_{\mathbb{R}^n} e^{-i\boldsymbol{x}.\boldsymbol{\eta}} f(\boldsymbol{x}) d\boldsymbol{x}. \tag{3.2}$$

We will mostly use the notation $\hat{f}(\boldsymbol{\eta}) := \mathcal{F}f(\boldsymbol{\eta})$.

The projections obtained from the electron microscope are mathematically expressed as integral transforms. They are well-defined on the so-called *Schwartz space*.

Definition 3.2. *The* Schwartz space $\mathcal{S}(\mathbb{R}^n)$ *is the linear space of functions $f \in C^\infty(\mathbb{R}^n)$ for which $\sup_{\boldsymbol{x}\in\mathbb{R}^n} = |\boldsymbol{x}^{\boldsymbol{\alpha}} D^{\boldsymbol{\beta}} f(\boldsymbol{x})| < \infty$ for all multiindices $\boldsymbol{\alpha}, \boldsymbol{\beta} \in \mathbb{N}_0^m$.*

Definition 3.3. *Let $f \in \mathcal{S}(\mathbb{R}^n), \boldsymbol{\theta} \in S^{n-1}$ and $s \in \mathbb{R}$, then the (n-dimensional)* Radon transform

$$\mathcal{R}f(\boldsymbol{\theta}, s) = \int_{\boldsymbol{x}.\boldsymbol{\theta}=s} f(\boldsymbol{x}) d\boldsymbol{x} = \int_{\boldsymbol{\theta}^\perp} f(s\boldsymbol{\theta} + \boldsymbol{y}) d\boldsymbol{y} \tag{3.3}$$

is the integral of f over the hyperplane perpendicular to $\boldsymbol{\theta}$ with distance $|s|$ from the origin.

Definition 3.4. *Let $f \in \mathcal{S}(\mathbb{R}^n), \boldsymbol{\theta} \in S^{n-1}$ and $\boldsymbol{x} \in \boldsymbol{\theta}^\perp \subset \mathbb{R}^n$, then the (n-dimensional)* X-ray transform *or* parallel beam transform

$$\mathcal{P}f(\boldsymbol{\theta}, \boldsymbol{x}) = \int_{-\infty}^{+\infty} f(\boldsymbol{x} + t\boldsymbol{\theta}) dt \tag{3.4}$$

is the integral of f over the straight line through $\boldsymbol{x}$ with direction $\boldsymbol{\theta}$. We call $\boldsymbol{\theta}$ the viewing direction.

The Radon and X-ray transform were defined on $\mathcal{S}(\mathbb{R}^n)$ above. However, we would like to extend them to $L^1(\mathbb{R}^n)$. The continuous functions with bounded support are dense in the space $L^1(\mathbb{R}^n)$. This means that for a function $f \in L^1(\mathbb{R}^n)$ we can find a sequence $f_n \in C(\mathbb{R}^n)$ with bounded support converging to f in the L^1-norm.
The Radon transform of f is then defined as the limit $\mathcal{R}f$ of the functions $\mathcal{R}f_n$ with respect to the L^1-norm. This limit satisfies

$$\int_{\mathbb{R}} |\mathcal{R}f(\boldsymbol{\theta}, s)| ds \leq \int_{\mathbb{R}^n} |f(\boldsymbol{x})| d\boldsymbol{x} < \infty$$

for all $\boldsymbol{\theta} \in S^{n-1}$. Fubini's theorem ensures that $\mathcal{R}f(\boldsymbol{\theta}, s)$ is well defined for almost every $(\boldsymbol{\theta}, s) \in S^{n-1} \times \mathbb{R}$. By the same argument this also holds for the X-ray transform. Thus the operators can be extended to $L^1(\mathbb{R}^n)$.

4. On viewing directions and object orientation

From now on we set $n = 3$ and denote by $f : \mathbb{R}^3 \to \mathbb{R}$ a three-dimensional density function. We assume that $f \in L^1(B) = \{f \in L^1(\mathbb{R}^3) \mid supp(f) \in B\}$, where B is the closed unit ball in $\mathbb{R}^3$. The viewing direction $\boldsymbol{\theta}$, defined in the X-ray transform as an element of S^2, can be uniquely described by two angles $\alpha \in [0, 2\pi)$ and $\beta \in [0, \pi]$ in spherical coordinates

$$\boldsymbol{\theta} = \boldsymbol{\theta}(\alpha, \beta) = \begin{pmatrix} \cos(\alpha)\sin(\beta) \\ \sin(\alpha)\sin(\beta) \\ \cos(\beta) \end{pmatrix}.$$

However, when the orientation of the object is unknown, a third variable must be introduced, specifying the rotation of the object relative to the viewing axis, i.e. the line in the viewing direction $\boldsymbol{\theta}$.

Euler Angles

The most practicable way to include the additional unknown component is to fix the viewing direction and look at a rotation $R \in SO(3)$ of the object, i.e. an orthogonal matrix with determinant 1. This leads to the following definition.

Definition 4.1. *The* projection of f at *projection orientation* $R \in SO(3)$ *in viewing*

direction x_3 is given by

$$\mathcal{P}(f,R)(x_1,x_2) = \int_{\mathbb{R}} f(R\boldsymbol{x})dx_3. \tag{4.1}$$

Since this is exactly the X-ray transform of the transformed density $f_R(\boldsymbol{x}) = f(R\boldsymbol{x})$ for $\theta = (0,0,1)$, we use the same notation. The third column $R^{(3)}$ of R will be referred to as the *projection direction.*
One way to describe such a matrix $R \in SO(3)$ are the so called *Euler angles.* The idea is to decompose the rotation into three elemental rotations about the axes of the coordinate system, corresponding to three angles (α,β,γ). We will look at

- counter-clockwise (the reference frame is right handed),
- active (the vector is rotated rather than the coordinate system),
- intrinsic (around the axes of the rotating reference frame)

rotations. Moreover, we will use the $z-y'-z''$ convention, meaning that we first do a rotation about the z-axis by α, then about the (new) y-axis by β and finally about the (new) z-axis by γ. This leads to the following definition.

Definition 4.2. *For a rotation matrix $R \in SO(3)$, the* Euler angles $\alpha \in [0,2\pi), \beta \in [0,\pi]$ *and* $\gamma \in [0,2\pi)$ *are given by the following equation.*

$$\begin{aligned} R &= R(\alpha)\cdot R(\beta)\cdot R(\gamma) \\ &= \begin{pmatrix} \cos(\alpha) & -\sin(\alpha) & 0 \\ \sin(\alpha) & \cos(\alpha) & 0 \\ 0 & 0 & 1 \end{pmatrix} \cdot \begin{pmatrix} \cos(\beta) & 0 & \sin(\beta) \\ 0 & 1 & 0 \\ -\sin(\beta) & 0 & \cos(\beta) \end{pmatrix} \cdot \begin{pmatrix} \cos(\gamma) & -\sin(\gamma) & 0 \\ \sin(\gamma) & \cos(\gamma) & 0 \\ 0 & 0 & 1 \end{pmatrix} \\ &= \begin{pmatrix} \cos(\alpha)\cos(\beta)\cos(\gamma) - \sin(\alpha)\sin(\gamma) & -\cos(\gamma)\sin(\alpha) - \cos(\alpha)\cos(\beta)\sin(\gamma) & \cos(\alpha)\sin(\beta) \\ \cos(\beta)\cos(\gamma)\sin(\alpha) + \cos(\alpha)\sin(\gamma) & \cos(\alpha)\cos(\gamma) - \cos(\beta)\sin(\alpha)\sin(\gamma) & \sin(\alpha)\sin(\beta) \\ -\cos(\gamma)\sin(\beta) & \sin(\beta)\sin(\gamma) & \cos(\beta) \end{pmatrix} \end{aligned}$$

We will denote this by $R = R(\alpha)R(\beta)R(\gamma) = R(\alpha,\beta,\gamma)$.

Note that the third column of R indeed is exactly the viewing direction defined in the X-ray transform.

5. Problem formulation

Given a set of projections $\{\mathcal{P}(f,R_i), i \in I\}$ for some index set I, we want to find the density function $f \in L^1(B)$ and the projection orientations $R_i \in SO(3)$, that is the

Euler angles $(\alpha_i, \beta_i, \gamma_i) \in [0, 2\pi) \times [0, \pi] \times [0, 2\pi)$ for all $i \in I$.
Denoting the data by $P_i(x_1, x_2)$, we get the following system of equations.

$$P_i(x_1, x_2) = \mathcal{P}(f, R_i)(x_1, x_2) = \int_{\mathbb{R}} f(R_i \boldsymbol{x}) dx_3 \tag{5.1}$$

for $i \in I$. The idea is to solve the problem in two steps. First the projection orientations R_i must be reconstructed. Once the orientation of the system is known, one can use inversion formulas of the X-ray transform to find f. This thesis is concerned with the first step, so we will discuss several techniques used to find the unknown orientations.

III. Common lines

The method of *common lines* is the most frequently used technique to reconstruct unknown projection orientations in three dimensions. *Common lines* were first mentioned in [CDK70, Appendix] and [Cro71] and were used for the reconstruction of symmetric particles. Later the concept was taken up again in [Hee87, "Angular Reconstitution"] and [Gon88a, "Geometric Method"], where also asymmetric particles were considered. In [Hee+97] an interesting overview of the history of *angular reconstitution* is given.

6. The Fourier Slice Theorem

The technique is based on the Fourier slice theorem, see for example [Nat01, Theorem 1.1], which states that the Fourier transform of the projection of an n-dimensional function onto an m-dimensional linear submanifold is equal to an m-dimensional central slice of the n-dimensional Fourier transform of that function. We begin with a version in $\mathbb{R}^3$ using the notion of orthogonal matrices and adopt the notation used in [SS12] and [SS11].

Theorem 6.1 (Fourier Slice Theorem 3D)**.** *Let $\boldsymbol{R}_i^{(1)}, \boldsymbol{R}_i^{(2)}$ and $\boldsymbol{R}_i^{(3)}$ denote the columns of a rotation matrix R_i and let $\boldsymbol{\eta} = (\eta_1, \eta_2, 0)$ and $\boldsymbol{u} = \left(\boldsymbol{R}_i^{(1)}, \boldsymbol{R}_i^{(2)}, \boldsymbol{R}_i^{(3)}\right)\boldsymbol{x} = R_i\boldsymbol{x}$. Then*

$$\hat{P}_i(\eta_1, \eta_2) = \sqrt{2\pi}\hat{f}(R_i\boldsymbol{\eta}). \tag{6.1}$$

Note that we take the two-dimensional Fourier transform on the left side and the three-dimensional Fourier transform on the right side.

Proof.

$$\begin{aligned}
\hat{P}_i(\eta_1, \eta_2) &= \frac{1}{2\pi} \iint_{\mathbb{R}^2} P_i(x_1, x_2) e^{i(x_1\eta_1 + x_2\eta_2)} dx_1 dx_2 \\
&= \frac{1}{2\pi} \iint_{\mathbb{R}^2} \left(\int_{\mathbb{R}} f(R_i\boldsymbol{x}) e^{i(\boldsymbol{\eta}\cdot\boldsymbol{x})} dx_3 \right) dx_1 dx_2 \\
&= \frac{1}{2\pi} \int_{\mathbb{R}^3} f(\boldsymbol{u}) e^{i\boldsymbol{\eta}\cdot(R_i^{\mathsf{T}}\boldsymbol{u})} d\boldsymbol{u}
\end{aligned}$$

$$= \frac{1}{2\pi} \int_{\mathbb{R}^3} f(\boldsymbol{u}) e^{i(R_i \boldsymbol{\eta}) \cdot \boldsymbol{u}} d\boldsymbol{u}$$
$$= (2\pi)^{1/2} \hat{f}(R_i \boldsymbol{\eta}) = (2\pi)^{1/2} \hat{f} \left(\eta_1 \boldsymbol{R}_i^{(1)} + \eta_2 \boldsymbol{R}_i^{(2)} \right).$$

□

This shows that the $2D-$Fourier transform of a projection onto the $x_1 - x_2-$plane with respect to the projection orientation R_i is exactly the $3D-$Fourier-transform of the object f evaluated on the plane spanned by $\boldsymbol{R}_i^{(1)}$ and $\boldsymbol{R}_i^{(2)}$, which is orthogonal to the projection direction $\boldsymbol{R}_i^{(3)}$.

Definition 6.2. *The plane spanned by $\boldsymbol{R}_i^{(1)}$ and $\boldsymbol{R}_i^{(2)}$ is often referred to as a* central section *as it goes through the origin. We denote it by*

$$C_i = \eta_1 \boldsymbol{R}_i^{(1)} + \eta_2 \boldsymbol{R}_i^{(2)}.$$

We now want to use the Fourier slice theorem again in two dimensions. This time we work with the Radon transform. We state the special case that the Fourier transform of the Radon transform of a projection is equal to the Fourier transform of that projection along a line through the origin.

Theorem 6.3 (Fourier Slice Theorem 2D)**.** *Let $\boldsymbol{\theta} \in S^1, \sigma \in \mathbb{R}$ and $P_i(x_1, x_1)$ be a projection of a density function f with projection orientation R_i. Then*

$$\widehat{\mathcal{R}P_i}(\boldsymbol{\theta}, \sigma) = \sqrt{2\pi}\, \widehat{P}_i(\sigma\boldsymbol{\theta}) \tag{6.2}$$

On the left side the one-dimensional Fourier transform is taken with respect to the second variable, while $\boldsymbol{\theta}$ is fixed and the two-dimensional Fourier transform is taken on the right side.

Proof. Let $\boldsymbol{\theta} = (\cos\varphi, \sin\varphi)$ and $t \in \mathbb{R}$. The *Radon transform* is then given by

$$\mathcal{R}f(\boldsymbol{\theta}, t) = \int_{\mathbb{R}} f\left(t \begin{pmatrix} \cos\varphi \\ \sin\varphi \end{pmatrix} + s \begin{pmatrix} -\sin\varphi \\ \cos\varphi \end{pmatrix} \right) ds.$$

The 2D Fourier transform gives

$$\widehat{P}_i(\sigma\boldsymbol{\theta}) = \frac{1}{2\pi} \int_{\mathbb{R}^2} P_i \begin{pmatrix} x_1 \\ x_2 \end{pmatrix} e^{i\sigma(x_1 \cos\varphi + x_2 \sin\varphi)} dx_1 dx_2. \tag{6.3}$$

We make a change of variables

$$\begin{pmatrix} x_1 \\ x_2 \end{pmatrix} = t\begin{pmatrix} \cos\varphi \\ \sin\varphi \end{pmatrix} + s\begin{pmatrix} -\sin\varphi \\ \cos\varphi \end{pmatrix},$$

where $dx_1 dx_2 = ds\ dt$ holds. So we get

$$\begin{aligned} \widehat{P}_i(\sigma\boldsymbol{\theta}) &= \frac{1}{2\pi}\int_{\mathbb{R}^2} P_i\begin{pmatrix} t\cos\varphi - s\sin\varphi \\ t\sin\varphi + s\cos\varphi \end{pmatrix} e^{i\sigma t} ds\ dt \\ &= \frac{1}{2\pi}\int_{\mathbb{R}}\left(\int_{\mathbb{R}} P_i\begin{pmatrix} t\cos\varphi - s\sin\varphi \\ t\sin\varphi + s\cos\varphi \end{pmatrix} ds\right) e^{i\sigma t} ds\ dt \\ &= \frac{1}{2\pi}\int_{\mathbb{R}} \mathcal{R}P_i(\boldsymbol{\theta}, t) e^{i\sigma t} dt \\ &= \frac{1}{\sqrt{2\pi}}\widehat{\mathcal{R}P_i}(\boldsymbol{\theta}, \sigma). \end{aligned} \tag{6.4}$$

□

Let us look at two different two-dimensional projections $P_i(x_1, x_2)$ and $P_j(x_1, x_2)$ given by X-ray transforms as in 3.4. In Fourier space each of them corresponds to a central section C_i and C_j respectively by the Fourier slice theorem 6.1,

$$\begin{aligned} \hat{P}_i(\eta_1, \eta_2) &= \sqrt{2\pi}\hat{f}\left(\eta_1 \boldsymbol{R}_i^{(1)} + \eta_2 \boldsymbol{R}_i^{(2)}\right), \\ \hat{P}_j(\eta_1, \eta_2) &= \sqrt{2\pi}\hat{f}\left(\eta_1 \boldsymbol{R}_j^{(1)} + \eta_2 \boldsymbol{R}_j^{(2)}\right). \end{aligned}$$

Being planes through the origin, those two central sections will intersect in one line going through the origin, called a central line. This means, we can find two directions $\boldsymbol{\theta}_i, \boldsymbol{\theta}_j \in S^1$, one in each central slice, such that

$$\hat{P}_i(\sigma\boldsymbol{\theta}_i) = \hat{P}_j(\sigma\boldsymbol{\theta}_j).$$

The Fourier slice theorem in two dimensions 6.3 says that we can find two angles $\varphi_1, \varphi_2 \in [0, 2\pi)$ defining this central line such that the Radon transforms in directions $\boldsymbol{\theta}_i = (\cos\varphi_i, \sin\varphi_i)$ and $\boldsymbol{\theta}_j = (\cos\varphi_j, \sin\varphi_j)$ of the two projections P_i and P_j coincide. This pair of angles is known as the *common line*, as in Fourier space it defines in fact a central line between two projections. This connection is depicted in figure 6.1.

Let us look at the concept in more detail. We look at the projections P_i and P_j in

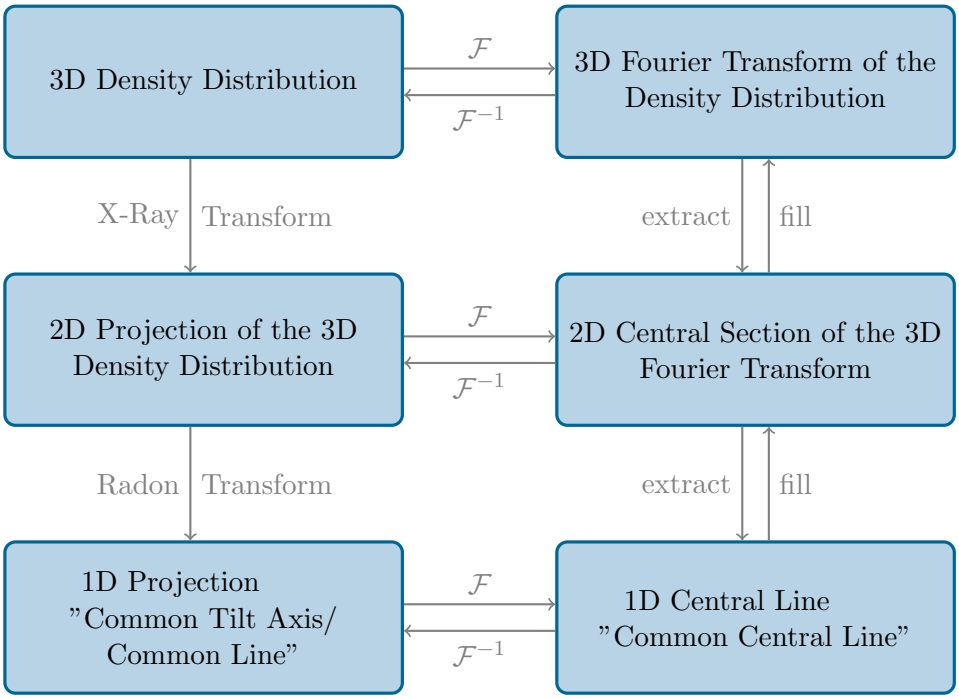

Figure 6.1.: The Fourier Slice Theorem

directions $\boldsymbol{R}_i^{(3)}$ and $\boldsymbol{R}_j^{(3)}$ and start with considering the unit vector

$$\boldsymbol{q}_{ij} = \frac{\left(\boldsymbol{R}_i^{(3)} \times \boldsymbol{R}_j^{(3)}\right)}{\left\|\boldsymbol{R}_i^{(3)} \times \boldsymbol{R}_j^{(3)}\right\|} \in S^2$$

in the direction of the common line. By definition it belongs to the planes $\boldsymbol{R}_i^{(3)} \cdot \boldsymbol{x} = 0$ and $\boldsymbol{R}_j^{(3)} \cdot \boldsymbol{x} = 0$ and we can write it in the orthonormal bases $\{\boldsymbol{R}_i^{(1)}, \boldsymbol{R}_i^{(2)}\}$ and $\{\boldsymbol{R}_j^{(1)}, \boldsymbol{R}_j^{(2)}\}$ as

$$\boldsymbol{q}_{ij} = \cos\psi_{ij}\boldsymbol{R}_i^{(1)} + \sin\psi_{ij}\boldsymbol{R}_i^{(2)} = \cos\psi_{ji}\boldsymbol{R}_j^{(1)} + \sin\psi_{ji}\boldsymbol{R}_j^{(2)} \tag{6.5}$$

for some angles $\psi_{ij}, \psi_{ji} \in [0, 2\pi)$. By construction, the Fourier transforms of the projections will coincide along the line with direction vector $\boldsymbol{q}_{ij}$, meaning for every

$t \in \mathbb{R}$

$$\begin{aligned}\hat{P}_i\left(t\cos\psi_{ij}, t\sin\psi_{ij}\right) &= \hat{f}\left(t\cos\psi_{ij}\boldsymbol{R}_i^{(1)} + t\sin\psi_{ij}\boldsymbol{R}_i^{(2)}\right)\\ &= \hat{f}\left(t\cos\psi_{ji}\boldsymbol{R}_j^{(1)} + t\sin\psi_{ji}\boldsymbol{R}_j^{(2)}\right)\\ &= \hat{P}_j\left(t\cos\psi_{ji}, t\sin\psi_{ji}\right).\end{aligned} \tag{6.6}$$

holds. We parametrise the common line by $\tilde{\boldsymbol{c_{ij}}} = (\cos\psi_{ij}, \sin\psi_{ij})$ in P_i and $\tilde{\boldsymbol{c_{ji}}} = (\cos\psi_{ji}, \sin\psi_{ji})$ in P_j and set

$$\boldsymbol{c_{ij}} = (\cos\psi_{ij}, \sin\psi_{ij}, 0), \qquad \boldsymbol{c_{ji}} = (\cos\psi_{ji}, \sin\psi_{ji}, 0).$$

Equation (6.5) can then be written in a short form as

$$\boldsymbol{q}_{ij} = R_i\boldsymbol{c_{ij}} = R_j\boldsymbol{c_{ji}}. \tag{6.7}$$

What is known in these calculations are the two projections P_i and P_j (i.e. the data) and the parametrisations $\tilde{\boldsymbol{c_{ij}}}$ and $\tilde{\boldsymbol{c_{ji}}}$ of the common line in the two projections. Those can be found by comparing all Radon transform in all directions from P_i with the Radon transforms of P_j and choose the directions $\tilde{\boldsymbol{c_{ij}}}$ and $\tilde{\boldsymbol{c_{ji}}}$ such that the transforms with respect to these directions coincide, see section 7. It is of course not clear, if there is a unique pair of directions or if the data is 'good enough' to compare the projections. We will discuss these problems later. For now we assume that everything can be determined uniquely.
Consequently the goal of the common line method is to determine the *relative orientations* of the projections, that is calculating the angles between the central sections (that correspond to the different projections) in Fourier space.
First we start with two different projections P_i and P_j. We know where the values on the planes $\hat{P}_i$ and $\hat{P}_j$ coincide and arbitrarily choose a line in three dimensional space to be this line of intersection. However, we do not know what the angle between the two planes is, see figure 6.2.

To get enough angular constraints to position the planes in space, we need to look at another projection P_k different from the first two projections. It will have a common line with P_i and a common line with P_j, meaning we know where the values on the planes $\hat{P}_k$ and $\hat{P}_i$ and the planes $\hat{P}_k$ and $\hat{P}_j$ coincide. In total we get three lines of intersection and the angles between them and know where to place the third central section in relation to the others, see figure 6.3. Hence we know the relative orientations

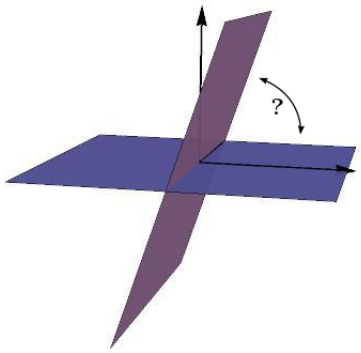

Figure 6.2.: Two planes $\hat{P}_i$ and $\hat{P}_j$ with known line of intersection.

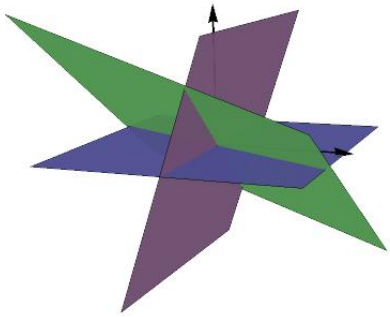

Figure 6.3.: Three planes $\hat{P}_i$, $\hat{P}_j$ and $\hat{P}_k$ with known lines of intersection.

of the projections and from those, we can compute the Euler angles that describe the rotation of the object, as we will see in subsection 6.1. Note that the alignment of the planes is not unique as a right- and a left-handed combination of the central sections are both correct solutions of the problem.

6.1. Calculation of the Euler angles

So far, we have talked about the idea of how to determine the relative orientations of the central sections in Fourier space, but we actually want to calculate for every projection P_i of the object f the rotation matrix R_i. In [Hee87] one can find the concrete computations. Remember that a rotation matrix is described by Euler angles as follows.

$$R_i = \begin{pmatrix} \cos(\alpha_i)\cos(\beta_i)\cos(\gamma_i) - \sin(\alpha_i)\sin(\gamma_i) & -\cos(\gamma_i)\sin(\alpha_i) - \cos(\alpha_i)\cos(\beta_i)\sin(\gamma_i) & \cos(\alpha_i)\sin(\beta_i) \\ \cos(\beta_i)\cos(\gamma_i)\sin(\alpha_i) + \cos(\alpha_i)\sin(\gamma_i) & \cos(\alpha_i)\cos(\gamma_i) - \cos(\beta_i)\sin(\alpha_i)\sin(\gamma_i) & \sin(\alpha_i)\sin(\beta_i) \\ -\cos(\gamma_i)\sin(\beta_i) & \sin(\beta_i)\sin(\gamma_i) & \cos(\beta_i) \end{pmatrix}.$$

In a first step we will recover the *projection direction*, that is the third column $\boldsymbol{R}_i^{(3)}$ of the matrix. Thus we can compute the Euler angles α and β. Only then we will calculate the remaining angle γ.
We denoted the direction of the common line by $\boldsymbol{q}_{ij}$ and wrote it in the orthonormal basis $\{\boldsymbol{R}_i^{(1)}, \boldsymbol{R}_i^{(2)}\}$ as follows $\boldsymbol{q}_{ij} = \cos\psi_{ij}\boldsymbol{R}_i^{(1)} + \sin\psi_{ij}\boldsymbol{R}_i^{(2)}$, see (6.5). As it is a unit vector, we can also write it in spherical coordinates

$$\boldsymbol{q}_{ij} = \begin{pmatrix} \cos\alpha_{ij}\sin\beta_{ij} \\ \sin\alpha_{ij}\sin\beta_{ij} \\ \cos\beta_{ij} \end{pmatrix}, \tag{6.8}$$

where $\alpha_{ij} \in [0, 2\pi)$ and $\beta_{ij} \in [0, \pi)$. Our goal is to compute for three projections P_i, P_j and P_k the directions of the common lines $\boldsymbol{q}_{ij}, \boldsymbol{q}_{ik}$ and $\boldsymbol{q}_{jk}$. Once we know them, we can compute the projection directions. Using that $\boldsymbol{R}_i^{(1)} \times \boldsymbol{R}_i^{(2)} = \boldsymbol{R}_i^{(3)}$ and that for two vectors $\boldsymbol{a}, \boldsymbol{b} \in \mathbb{R}^3$ $\boldsymbol{a} \times \boldsymbol{a} = 0$ and $\boldsymbol{a} \times \boldsymbol{b} = -\boldsymbol{b} \times \boldsymbol{a}$ holds true, we get

$$\begin{aligned} \boldsymbol{q}_{ij} \times \boldsymbol{q}_{ik} &= \left(\cos\psi_{ij}\boldsymbol{R}_i^{(1)} + \sin\psi_{ij}\boldsymbol{R}_i^{(2)}\right) \times \left(\cos\psi_{ik}\boldsymbol{R}_i^{(1)} + \sin\psi_{ik}\boldsymbol{R}_i^{(2)}\right) \\ &= \cos\psi_{ij}\sin\psi_{ik}\left(\boldsymbol{R}_i^{(1)} \times \boldsymbol{R}_i^{(2)}\right) + \sin\psi_{ij}\cos\psi_{ik}\left(\boldsymbol{R}_i^{(2)} \times \boldsymbol{R}_i^{(1)}\right) \\ &= \cos\psi_{ij}\sin\psi_{ik}\boldsymbol{R}_i^{(3)} + \sin\psi_{ij}\cos\psi_{ik}\left(-\boldsymbol{R}_i^{(3)}\right) \\ &= \left(\cos\psi_{ij}\sin\psi_{ik} - \sin\psi_{ij}\cos\psi_{ik}\right)\boldsymbol{R}_i^{(3)} \\ &= \sin\left(\psi_{ik} - \psi_{ij}\right)\boldsymbol{R}_i^{(3)}. \end{aligned} \tag{6.9}$$

This equation does not lead to a solution if $\sin(\psi_{ik} - \psi_{ij}) = 0$, so whenever $\psi_{ik} - \psi_{ij} = 0$ or $\psi_{ik} - \psi_{ij} = \pi$. This is the case, if the common lines of P_i with P_j and P_i with P_k coincide and we have $\boldsymbol{q}_{ij} = \pm\boldsymbol{q}_{ik}$. However, we have assumed that the three different projections are different (not only as far as the direction is concerned, but also regarding the projection itself), and hence this situation will not occur. In total,

after similar calculations for the other two projection directions, this leads to

$$\begin{aligned} \boldsymbol{R}_i^{(3)} &= \frac{\boldsymbol{q}_{ij} \times \boldsymbol{q}_{ik}}{\sin\left(\psi_{ik} - \psi_{ij}\right)}, \\ \boldsymbol{R}_j^{(3)} &= \frac{\boldsymbol{q}_{ij} \times \boldsymbol{q}_{jk}}{\sin\left(\psi_{jk} - \psi_{ji}\right)}, \\ \boldsymbol{R}_k^{(3)} &= \frac{\boldsymbol{q}_{ik} \times \boldsymbol{q}_{jk}}{\sin\left(\psi_{kj} - \psi_{ki}\right)}. \end{aligned} \tag{6.10}$$

Let us now find the directions of the common lines $\boldsymbol{q}_{ij}, \boldsymbol{q}_{ik}$ and $\boldsymbol{q}_{jk}$. The vector entries or angles we already know are denoted in green. First of all, the relative orientations of the three projections are fixed, whereas the absolute orientation of the object relative to the coordinate system is arbitrary and may be chosen freely. We therefore choose the common tilt axis $\boldsymbol{q}_{ij}$ to coincide with the z-axis,

$$\boldsymbol{q}_{ij} = \begin{pmatrix} 0 \\ 0 \\ 1 \end{pmatrix}.$$

In view of definition 6.8, we have $\beta_{ij} = 0$. Next, we choose the common line $\boldsymbol{q}_{ik}$ to lie in the y-z-plane, i.e. the first component vanishes and we can set $\alpha_{ik} = \frac{\pi}{2}$. Thus

$$\boldsymbol{q}_{ik} = \begin{pmatrix} 0 \\ \sin\beta_{ik} \\ \cos\beta_{ik} \end{pmatrix}.$$

For the third common tilt axis we still have

$$\boldsymbol{q}_{jk} = \begin{pmatrix} \cos\alpha_{jk}\sin\beta_{jk} \\ \sin\alpha_{jk}\sin\beta_{jk} \\ \cos\beta_{jk} \end{pmatrix}.$$

What we know from the data as well, are the angles between the common tilt axis, since

$$\begin{aligned} \boldsymbol{q}_{ij} \cdot \boldsymbol{q}_{ik} &= \left(\cos\psi_{ij}\boldsymbol{R}_i^{(1)} + \sin\psi_{ij}\boldsymbol{R}_i^{(2)}\right) \cdot \left(\cos\psi_{ik}\boldsymbol{R}_i^{(1)} + \sin\psi_{ik}\boldsymbol{R}_i^{(2)}\right) \\ &= \cos\psi_{ij}\cos\psi_{ik} + \sin\psi_{ij}\sin\psi_{ik} \\ &= \cos\left(\psi_{ij} - \psi_{ik}\right), \end{aligned} \tag{6.11}$$

where we use the relations $\boldsymbol{R}_i^{(2)} \cdot \boldsymbol{R}_i^{(2)} = 1$ and $\boldsymbol{R}_i^{(1)} \cdot \boldsymbol{R}_i^{(2)} = 0$ for the columns of a

rotation matrix. Hence, we get the additional equations

$$\begin{aligned}
\cos(\psi_{ij} - \psi_{ik}) &= \boldsymbol{q}_{ij} \cdot \boldsymbol{q}_{ik} = \cos\beta_{ik}, \\
\cos(\psi_{ji} - \psi_{jk}) &= \boldsymbol{q}_{ij} \cdot \boldsymbol{q}_{jk} = \cos\beta_{jk}, \\
\cos(\psi_{ki} - \psi_{kj}) &= \boldsymbol{q}_{ik} \cdot \boldsymbol{q}_{jk} = \sin\beta_{ik} \sin\alpha_{jk} \sin\beta_{jk} + \cos\beta_{ik} \cos\beta_{jk}.
\end{aligned} \tag{6.12}$$

As we know $\cos\beta_{ik}$ and $\cos\beta_{jk}$, we can derive values for $\sin\beta_{ik}$ and $\sin\beta_{jk}$. However, there is no unique way to do this, because we don't know the angles β_{ik} and β_{jk}. Both, $\sin\beta_{ik}$ and $\sin(2\pi - \beta_{ik})$ are possible choices, see figure 6.4, so as already mentioned before, we see that the alignment of the planes is only unique up to handedness. At this

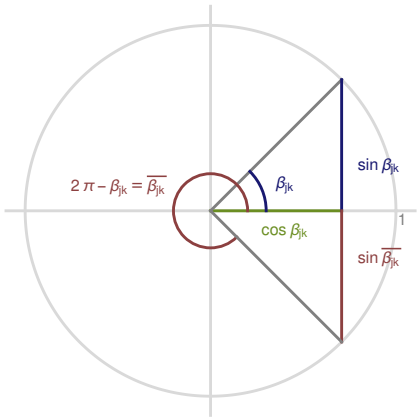

Figure 6.4.: The situation depicted in the unit circle.

point everything except $\sin\alpha_{jk}$ and $\cos\alpha_{jk}$ is known, but now that we have decided for certain values of $\sin\beta_{ik}$ and $\sin\beta_{jk}$, we can solve the third equation in 6.12 for $\sin\alpha_{jk}$ and choose some $\cos\alpha_{jk}$. Again, we can not determine the values uniquely.
In sum we have the following solution, where the directly known entries are denoted in green and the non-unique entries we have chosen are denoted in red.

$$\boldsymbol{q}_{ij} = \begin{pmatrix} 0 \\ 0 \\ 1 \end{pmatrix}$$

$$\boldsymbol{q}_{ik} = \begin{pmatrix} 0 \\ \sin\beta_{ik} \\ \cos\beta_{ik} \end{pmatrix} = \begin{pmatrix} 0 \\ \sin(\psi_{ij} - \psi_{ik}) \\ \cos(\psi_{ij} - \psi_{ik}) \end{pmatrix}$$

$$\boldsymbol{q}_{jk} = \begin{pmatrix} \cos\alpha_{jk}\sin\beta_{jk} \\ \sin\alpha_{jk}\sin\beta_{jk} \\ \cos\beta_{jk} \end{pmatrix} = \begin{pmatrix} \cos\alpha_{jk}\sin\left(\psi_{ji}-\psi_{jk}\right) \\ \frac{\cos\left(\psi_{ki}-\psi_{kj}\right)-\cos(\psi_{ij}-\psi_{ik})\cos\left(\psi_{ji}-\psi_{jk}\right)}{\sin(\psi_{ij}-\psi_{ik})} \\ \cos\left(\psi_{ji}-\psi_{jk}\right) \end{pmatrix}$$

Using equations 6.10 it is now possible to compute the third columns of the rotations matrices R_i, R_j and R_k and hence the Euler angles $\alpha_i, \alpha_j, \alpha_k, \beta_i, \beta_j$ and β_k.

Finally, we want to find the remaining angles γ_i, γ_j and γ_k. Using equation 6.7 and the notation $R_i = R(\alpha_i) \cdot R(\beta_i) \cdot R(\gamma_i)$ for all rotation matrices, we have

$$\begin{aligned} R(\gamma_i)\boldsymbol{c}_{ij} &= \left(R(\alpha_i)\cdot R(\beta_i)\right)^{-1}\boldsymbol{q}_{ij} \\ R(\gamma_j)\boldsymbol{c}_{jk} &= \left(R(\alpha_j)\cdot R(\beta_j)\right)^{-1}\boldsymbol{q}_{jk} \\ R(\gamma_k)\boldsymbol{c}_{ki} &= \left(R(\alpha_k)\cdot R(\beta_k)\right)^{-1}\boldsymbol{q}_{ik} \end{aligned} \tag{6.13}$$

We know the directions of the common lines $\boldsymbol{c}_{**}$ in the real space coordinate system and moreover, we already calculated the directions of the common lines $\boldsymbol{q}_{**}$ in Fourier space and the Euler angles α_* and β_*. Therefore, we get a system of equations for $\cos\gamma_*$ and $\sin\gamma_*$ and can determine the missing angles.

6.2. An easy example

Let us look at an example that Van Heel discussed in [Hee87] and apply the method of common lines to a simple object consisting of twelve balls, see figure 6.5. A class of particles with similar symmetries are for instance oligomeric enzymes, see [MB73].

We have given three projections P_1, P_2 and P_3 of the balls (figure 6.6) and want to

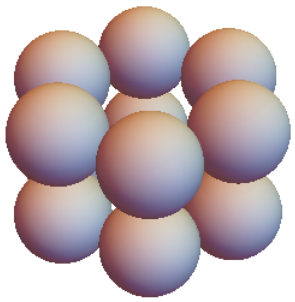

Figure 6.5.: Twelve balls in D6 symmetry.

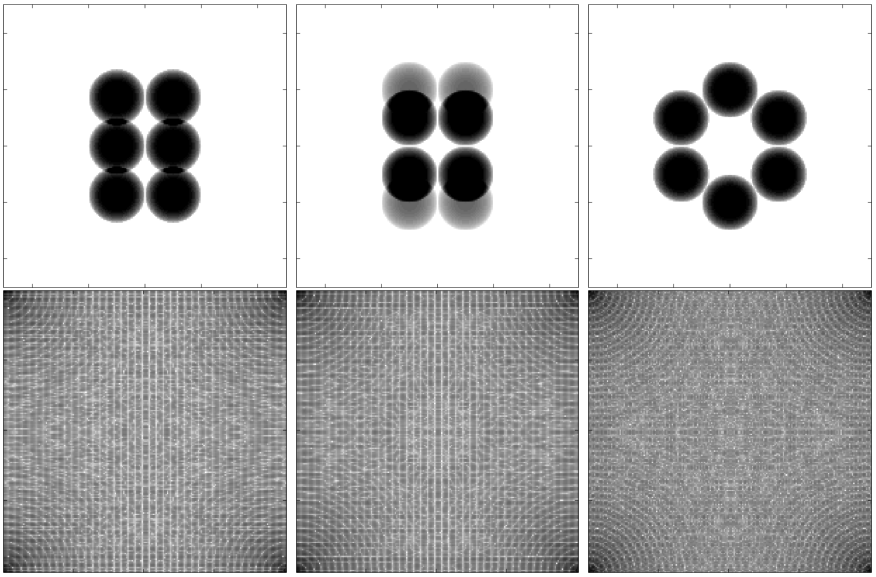

Figure 6.6.: The projections P_1, P_2 and P_3 in the first and the logarithm of the magnitude of their Fourier transforms in the second line.

recover the rotation matrices R_1, R_2 and R_3. We will do this step by step as described above.

Common line data

In subsection 7.1 the methods for line detection are demonstrated by the example of the van Heel balls. In this example the data is quite simple and we can spot possible projection directions defining the common line with the naked eye. The following values are assumed to be given

$$\begin{aligned}
\tilde{\boldsymbol{c}}_{12} &= (\cos\psi_{12}, \sin\psi_{12}) = (1,0) \Rightarrow \psi_{12} = 0 \\
\tilde{\boldsymbol{c}}_{21} &= (\cos\psi_{21}, \sin\psi_{21}) = (1,0) \Rightarrow \psi_{21} = 0 \\
\tilde{\boldsymbol{c}}_{13} &= (\cos\psi_{13}, \sin\psi_{13}) = (0,1) \Rightarrow \psi_{13} = \frac{\pi}{2} \\
\tilde{\boldsymbol{c}}_{31} &= (\cos\psi_{31}, \sin\psi_{31}) = (1,0) \Rightarrow \psi_{31} = 0 \\
\tilde{\boldsymbol{c}}_{23} &= (\cos\psi_{23}, \sin\psi_{23}) = (0,1) \Rightarrow \psi_{23} = \frac{\pi}{2} \\
\tilde{\boldsymbol{c}}_{32} &= (\cos\psi_{32}, \sin\psi_{32}) = (0,1) \Rightarrow \psi_{32} = \frac{\pi}{2}
\end{aligned} \tag{6.14}$$

Common lines in Fourier space

As in the general setting we choose the first common line to coincide with the $z-$axis

$$\boldsymbol{q}_{12} = \begin{pmatrix} 0 \\ 0 \\ 1 \end{pmatrix},$$

and the second one to lie in the $y-z-$plane

$$\boldsymbol{q}_{13} = \begin{pmatrix} 0 \\ \sin\beta_{13} \\ \cos\beta_{13} \end{pmatrix},$$

while the third one is given by

$$\boldsymbol{q}_{23} = \begin{pmatrix} \cos\alpha_{23}\sin\beta_{23} \\ \sin\alpha_{23}\sin\beta_{23} \\ \cos\beta_{23} \end{pmatrix}.$$

For the remaining angles we use the equations in 6.12 and get

$$\begin{aligned} \cos\beta_{13} &= \cos\left(\psi_{12} - \psi_{13}\right) = \cos\left(-\frac{\pi}{2}\right) = 0, \\ \cos\beta_{23} &= \cos\left(\psi_{21} - \psi_{23}\right) = \cos\left(-\frac{\pi}{2}\right) = 0, \\ \sin\alpha_{23} &= \frac{\cos\left(\psi_{31} - \psi_{32}\right) - \cos\beta_{13}\cos\beta_{23}}{\sin\beta_{13}\sin\beta_{23}} = \cos\left(-\frac{\pi}{2}\right) = 0, \end{aligned} \tag{6.15}$$

so $\sin\beta_{13} = 1$, $\sin\beta_{23} = 1$ and $\cos\beta_{23} = 1$. Therefore the common lines are given by

$$\boldsymbol{q}_{12} = \begin{pmatrix} 0 \\ 0 \\ 1 \end{pmatrix}, \qquad \boldsymbol{q}_{13} = \begin{pmatrix} 0 \\ 1 \\ 0 \end{pmatrix}, \qquad \boldsymbol{q}_{23} = \begin{pmatrix} 1 \\ 0 \\ 0 \end{pmatrix}.$$

We now see that, with the choices we made, the central sections intersect exactly at the axes in Fourier space (see figure 6.7).

Euler angles α and β

Using equations 6.10 it is possible to compute the third columns of the rotation matrices $\boldsymbol{R}_1^{(3)}, \boldsymbol{R}_2^{(3)}$ and $\boldsymbol{R}_3^{(3)}$ and from these vectors the first two Euler angles. We

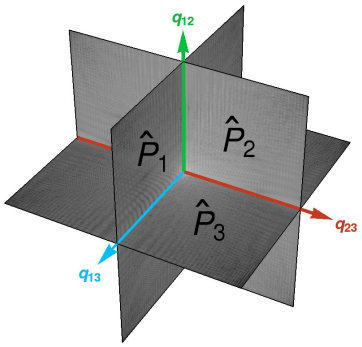

Figure 6.7.: The squared magnitudes of the (discrete) Fourier transforms of the projections, i.e. the power spectra, are placed according to the computed common lines in space.

have

$$\boldsymbol{R}_1^{(3)} = \frac{\boldsymbol{q}_{12} \times \boldsymbol{q}_{13}}{\sin\left(\psi_{13} - \psi_{12}\right)} = \frac{1}{\sin\left(\frac{\pi}{2}\right)} \begin{pmatrix} 0 \\ 0 \\ 1 \end{pmatrix} \times \begin{pmatrix} 0 \\ 1 \\ 0 \end{pmatrix} = \begin{pmatrix} -1 \\ 0 \\ 0 \end{pmatrix},$$

$$\boldsymbol{R}_2^{(3)} = \frac{\boldsymbol{q}_{12} \times \boldsymbol{q}_{23}}{\sin\left(\psi_{23} - \psi_{21}\right)} = \frac{1}{\sin\left(\frac{\pi}{2}\right)} \begin{pmatrix} 0 \\ 0 \\ 1 \end{pmatrix} \times \begin{pmatrix} 1 \\ 0 \\ 0 \end{pmatrix} = \begin{pmatrix} 0 \\ 1 \\ 0 \end{pmatrix},$$

$$\boldsymbol{R}_3^{(3)} = \frac{\boldsymbol{q}_{13} \times \boldsymbol{q}_{23}}{\sin\left(\psi_{32} - \psi_{31}\right)} = \frac{1}{\sin\left(\frac{\pi}{2}\right)} \begin{pmatrix} 0 \\ 1 \\ 0 \end{pmatrix} \times \begin{pmatrix} 1 \\ 0 \\ 0 \end{pmatrix} = \begin{pmatrix} 0 \\ 0 \\ -1 \end{pmatrix},$$

and therefore get the following equations for the angles $\alpha_* \in [0, 2\pi)$ and $\beta_* \in [0, \pi]$

$$\boldsymbol{R}_1^{(3)} = \begin{pmatrix} \cos\alpha_1 \sin\beta_1 \\ \sin\alpha_1 \sin\beta_1 \\ \cos\beta_1 \end{pmatrix} = \begin{pmatrix} -1 \\ 0 \\ 0 \end{pmatrix},$$
$$\boldsymbol{R}_2^{(3)} = \begin{pmatrix} \cos\alpha_2 \sin\beta_2 \\ \sin\alpha_2 \sin\beta_2 \\ \cos\beta_2 \end{pmatrix} = \begin{pmatrix} 0 \\ 1 \\ 0 \end{pmatrix},$$
$$\boldsymbol{R}_3^{(3)} = \begin{pmatrix} \cos\alpha_3 \sin\beta_3 \\ \sin\alpha_3 \sin\beta_3 \\ \cos\beta_3 \end{pmatrix} = \begin{pmatrix} 0 \\ 0 \\ -1 \end{pmatrix}.$$

In this case the following angles can be determined uniquely.

$$\beta_1 = \frac{\pi}{2}, \qquad \alpha_1 = \pi,$$
$$\beta_2 = \frac{\pi}{2}, \qquad \alpha_2 = \frac{\pi}{2},$$
$$\beta_3 = \pi.$$

As for α_3 any value satisfies the equations above and we choose it to be zero, $\alpha_3 = 0$. Remember that we look at intrinsic rotations, so the the rotations are made with respect to a rotating reference frame. The reason why α_3 is arbitrary here is that the first z-axis we rotate about (by α_3) and the new z-axis we rotate about (by γ_3) have the same direction. This means we can only recover the difference $\alpha_3 - \gamma_3$.

Euler angle γ

Finally, we use 6.13 and get for $\gamma_* \in [0, 2\pi)$

$$\cos\gamma_1 = -1, \qquad \cos\gamma_2 = -1, \qquad \cos\gamma_3 = 0,$$
$$\sin\gamma_1 = 0, \qquad \sin\gamma_2 = 0, \qquad \sin\gamma_3 = 1.$$

Thus, $\gamma_1 = \gamma_2 = \pi$ and $\gamma_3 = \frac{\pi}{2}$. The final result is

$$R_1 = R\left(\pi, \frac{\pi}{2}, \pi\right), \qquad R_2 = R\left(\frac{\pi}{2}, \frac{\pi}{2}, \pi\right), \qquad R_3 = R\left(0, \pi, \frac{\pi}{2}\right).$$

7. Methods for line detection

In this section we will discuss several methods for finding the directions of the common lines, which we have so far assumed to be given already.

7.1. Cross Correlation

Introduced in [Hee87] as well, the idea of cross correlation (CC) is to compare each one-dimensional projection of one two-dimensional projection with all one-dimensional projections of another two-dimensional projection in order to find the directions of the common line between those two two-dimensional projections. In order to compare functions the cross correlation coefficient, see for example [Bra78], is used.

Definition 7.1. *Let $g_1, g_2 \in L^2(\mathbb{R})$, then the* normalised cross correlation coefficient *is defined as follows*

$$CCC(g_1, g_2)(\tau) = \frac{\int_{\mathbb{R}} g_1(t) g_2(t+\tau) dt}{\|g_1\|_{L^2(\mathbb{R})} \|g_2\|_{L^2(\mathbb{R})}}. \tag{7.1}$$

The variable τ is the displacement, also known as lag. *The coefficient takes values between -1 and 1 and is maximised when the functions g_1 and g_2 coincide, see figure 7.1.*

Let us now look at two different projections P_1 and P_2 of the same object and their sinograms, that is the two dimensional Radon transform data, see for example figure 7.2. We want to compare all the line integrals in some fixed direction ϕ of the first projection P_1 with all the line integrals in another fixed direction ϑ of the second projection P_2 respectively. Speaking in terms of the sinograms, we want to compare the column at position ϕ in the sinogram of P_1 with the column at position ϑ in the sinogram of the second projection P_2. We can use the correlation coefficient to get a measure of identicalness, namely the *sinogram correlation function (SCF)*, as can be found in [Hee87], [Hee+00] and [Hee+97].

$$SCF_{12}(\phi, \vartheta) = CCC(\mathcal{R}_\phi P_1, \mathcal{R}_\vartheta P_2)(0) = \frac{\int_{\mathbb{R}} \mathcal{R}_\phi P_1(s) \mathcal{R}_\vartheta P_2(s) ds}{\|\mathcal{R}_\phi P_1\|_{L^2(\mathbb{R})} \|\mathcal{R}_\vartheta P_2\|_{L^2(\mathbb{R})}}.$$

Since we do not want to find the best match of the two functions for a certain displacement, but just an indicator for the correlation, we set the displacement variable τ to zero.
In order to find the common line between the two projections, we can compute the

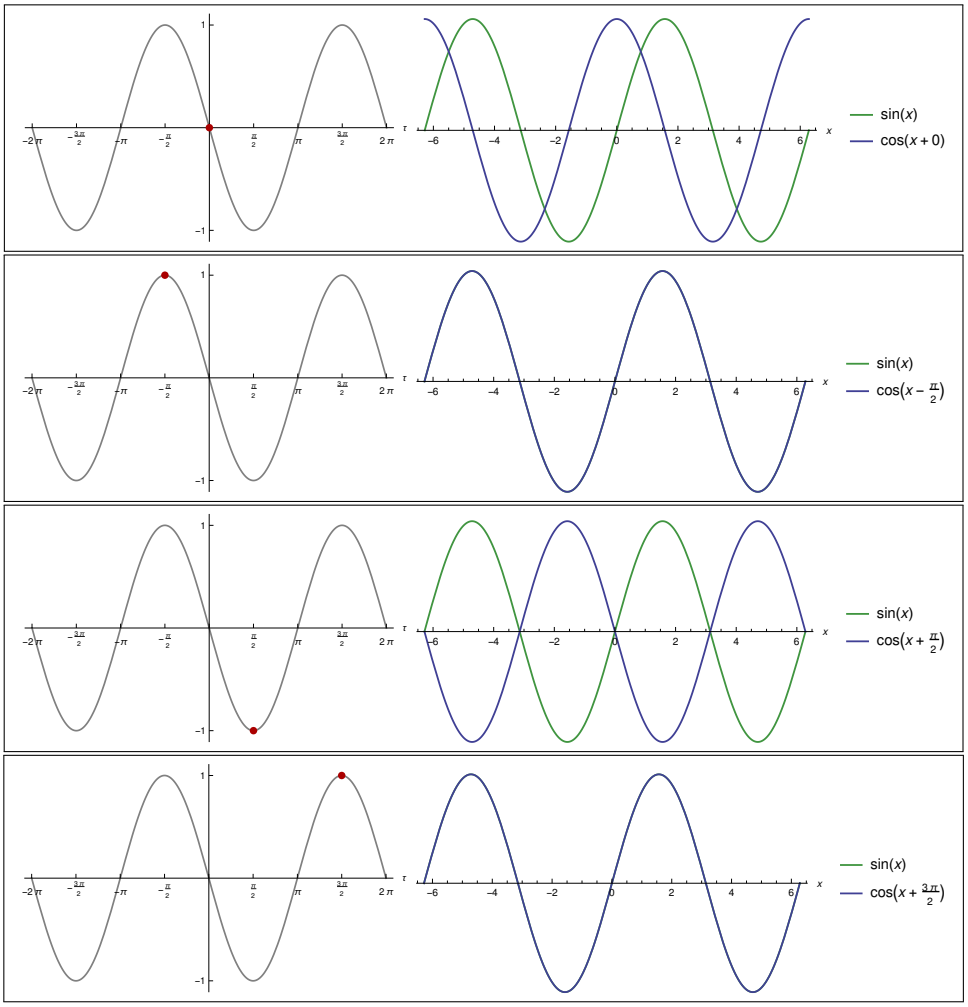

Figure 7.1.: On the left side the normalized cross correlation of the two functions is depicted, whereas on the right side $sin(x)$ and a shifted $cos(x)$ are plotted. For a shift of $\frac{-\pi}{2}$ and $\frac{3\pi}{2}$ (second and fourth line) the sine and cosine function coincide and the correlation has a maximum. If the displacement equals $\frac{\pi}{2}$ (third line) the functions differ from each other the most and the correlation coefficient has a minimum.

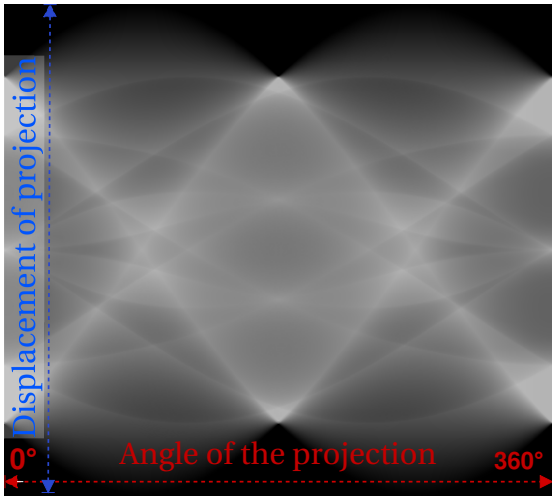

Figure 7.2.: Sinogram of the first projection of the twelve balls from the previous section. The x-direction corresponds to the angle of the Radon transform and the y-direction shows the displacement of the Radon transform.

values of the correlation coefficient for all angles ϕ and ϑ, as can be seen in the example of the van Heel balls (figures 7.4,7.5 and 7.6). A maximum of the sinogram correlation function will indicate a high correlation and hence will lead to two angles defining a common line.

Mutual correlation

When using cross correlation functions it happens that strong frequency components in the data dominate the weaker components, that is typically the high-frequency ones associated with information of the particles we are interested in. To address this problem, in [HSO92] the *mutual correlation function*, which is essentially a version of cross correlation coefficient from which the square root is taken, is introduced. In this case, the *amplitude square root filtered* version of the object density is used.

Van Heel Balls Revisited

We go back to the example in section 6.2, where we have assumed the directions of the Radon transforms defining the common lines are known 6.14. To see that these values are actually a proper choice, we will look at the sinograms, see figure 7.3, of the projections and calculate the sinogram correlation functions.

In order to get a good overview of what is happening, we include the corresponding

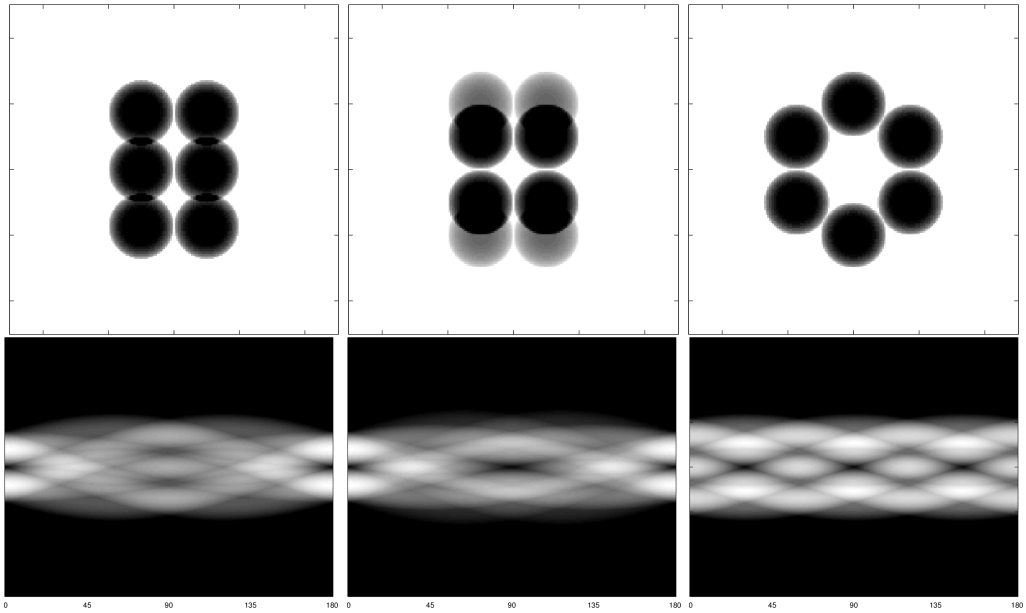

Figure 7.3.: In the first line the projections P_1, P_2 and P_3 are shown again. In the second line the corresponding sinograms are depicted.

projections and their sinograms on the bottom and the right side of the figures 7.4,7.5 and 7.6. In the center the sinogram correlation functions SCF are shown. The white or lighter spots indicate high correlation between the corresponding columns in the sinograms, while black or darker areas mean that there is no or bad correlation. The angles chosen for the calculations in section 6.2 are marked with a red star.

In all SCFs there are several possible choices for angles defining the common lines. That is due to to the symmetry of the object. When the symmetry is known, this can be taken into account when choosing the angles. However in general, if there are non-trivial symmetries and no prior information about the object is available, interpreting the SCF can be fairly difficult.

7.2. Least squares

Very similar to cross correlation is the method of least squares (LS) [Gon90; Gon88b; PZF96; SS11]. The idea is to minimize the integral over the squared differences between the Radon transforms of the first projection P_1 and the Radon transforms of the second projection P_2 over all possible directions ϕ and ϑ

$$\min_{\phi,\vartheta\in[0,2\pi)} \int_{\mathbb{R}} |\mathcal{R}_\phi P_1(s) - \mathcal{R}_\vartheta P_2(s)|^2 ds. \tag{7.2}$$

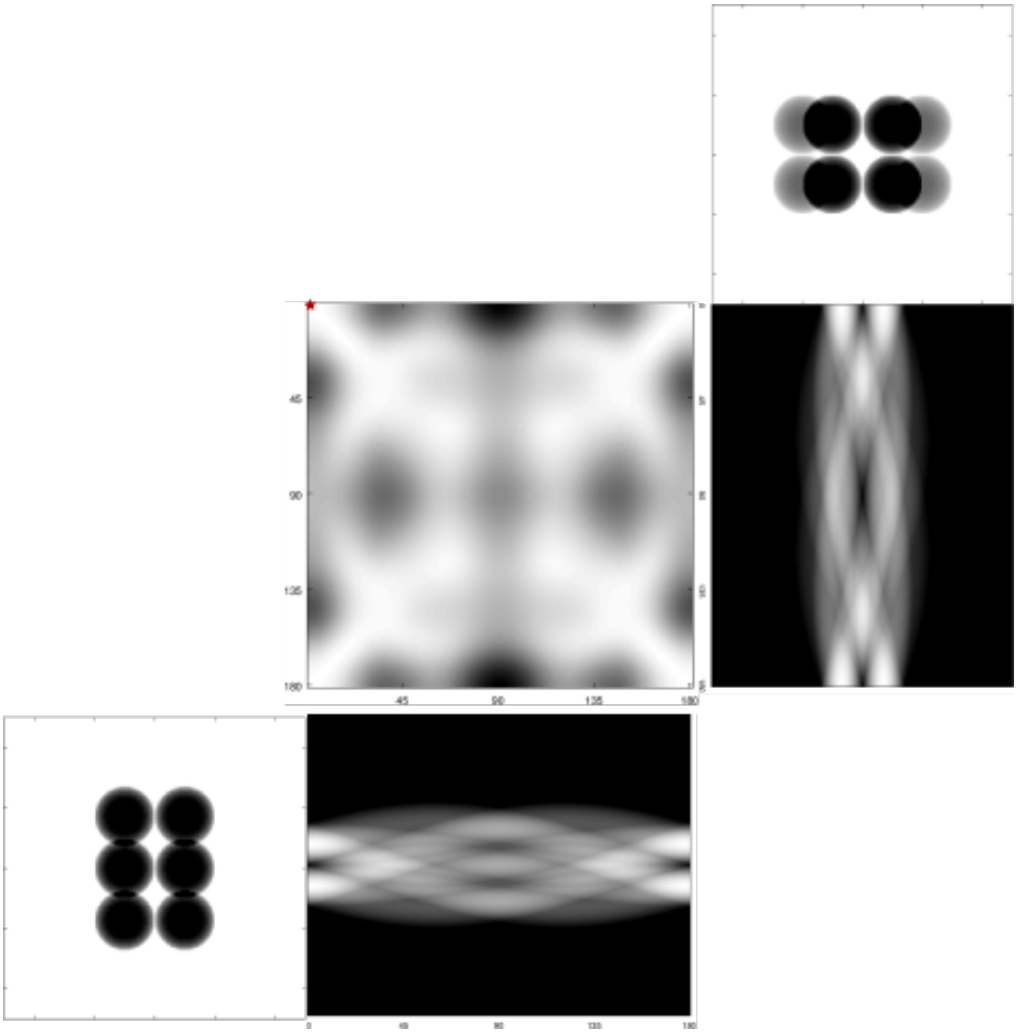

Figure 7.4.: **Sinogram Correlation Function for the projections P_1 and P_2.** On the bottom the projection P_1 and its sinogram are depicted while on the right side we can see the projection P_2 and its sinogram rotated by 90 degrees. The angles that have been chosen for our calculations are $\psi_{12} = \psi_{21} = 0$.

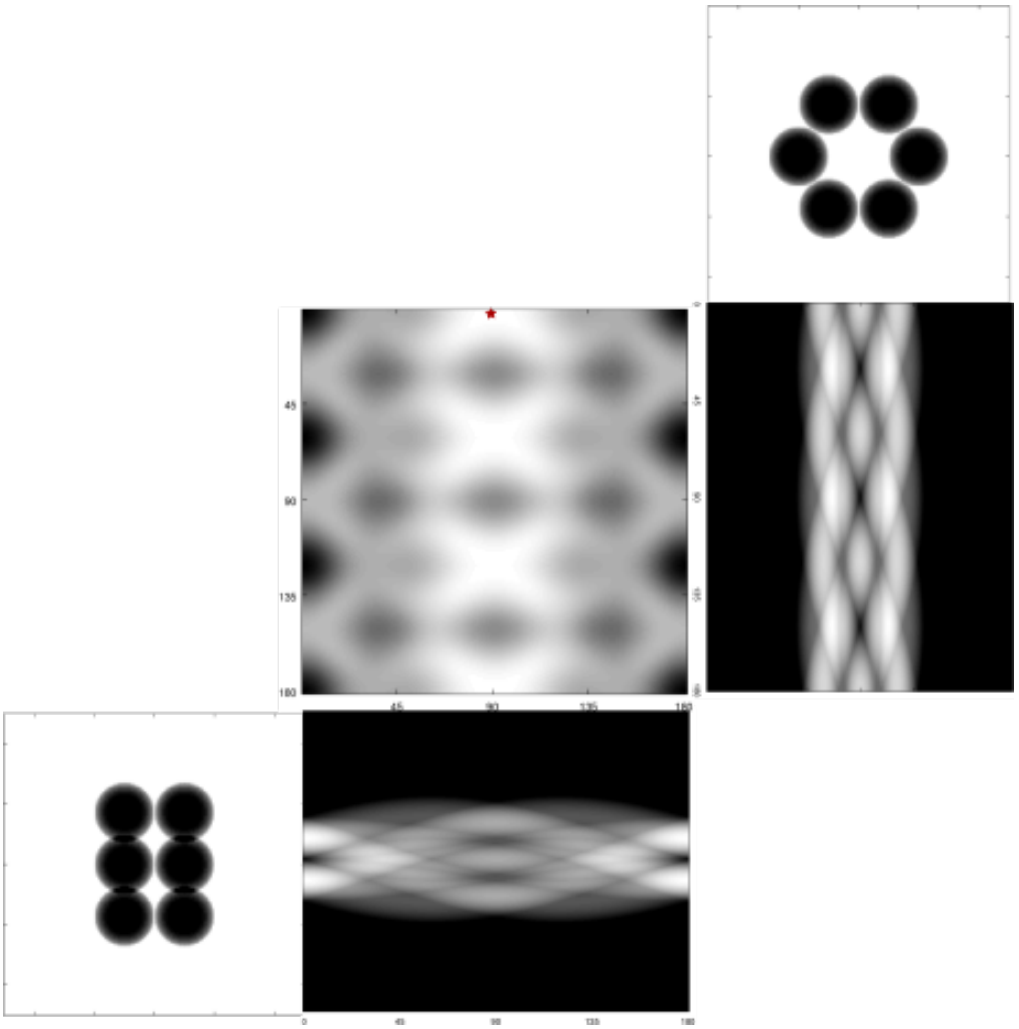

Figure 7.5.: **Sinogram Correlation Function for the projections P_1 and P_3.** The angles that have been chosen for our calculations are $\psi_{13} = \frac{\pi}{2}$ and $\psi_{31} = 0$.

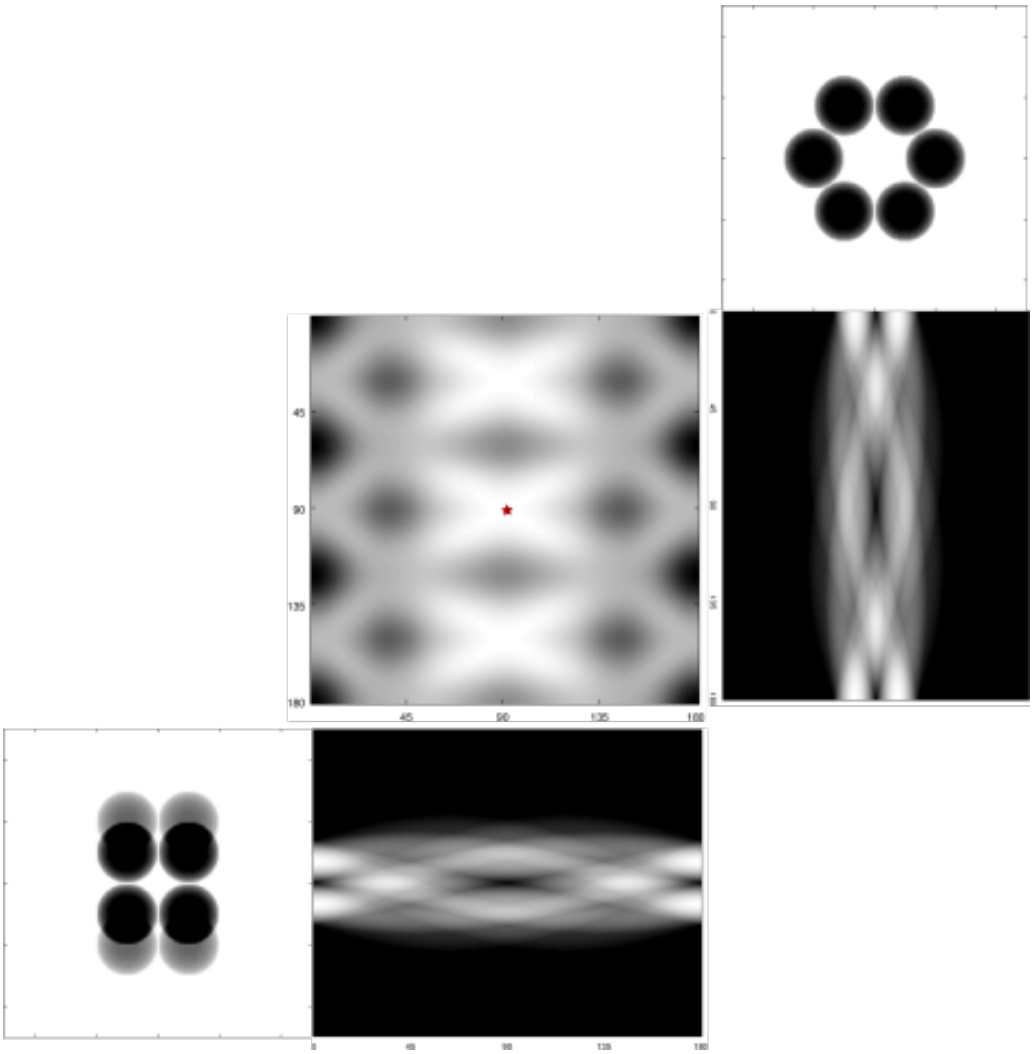

Figure 7.6.: **Sinogram Correlation Function for the projections P_2 and P_3.** The angles that have been chosen for our calculations are $\psi_{23} = \frac{\pi}{2}$ and $\psi_{32} = \frac{\pi}{2}$.

7.3. Other techniques

The methods using the cross correlation coefficient and least squares approximations, respectively, often suffer from low common line detection rates due to noisy images, eventually leading to inconclusive values for the projection directions. Addressing this problem some strategies were developed to improve the quality of the CC or LS method. Mallick at al. [Mal+06] use a Bayesian approach to denoise a matrix containing the angles obtained by minimizing the differences between the Radon transforms in all possible directions of the two-dimensional projections. Singer et al. [Sin+10] established a voting procedure to determine which common line pairs were detected correctly.
Other methods for solving the optimization problem to find the common lines in the first place include eigenvectors and semidefinite programming [SS11; HS11; WSW13] or synchronization [SS12]. They all have the shared aim of reducing the sensitivity of the common line detection to noise and therefore enhancing the quality of the three-dimensional reconstruction.

8. Exploiting Symmetry

An assumption we have made in the description of the method is that, if we have a projection of an object, it originates from only one projection direction. In other words we have assumed to deal with an asymmetric object. A lot of particles, in fact including the simple example of the *van Heel balls*, have certain symmetries. Examples would be the *hibiscus chlorotic ringspot virus* [Doa+03], an icosahedral virus particle, or the *lumbricus terrestris hemoglobin* molecule [Sch+95]. As mentioned in the introduction to this chapter, the method of common lines was even introduced to deal with symmetric particles first [Cro71]. If the symmetry is known, it is indeed easier to solve the problem as the three independent projections required might already be present in one single projection and the search process for orientation determination can be restricted to a relatively small angular domain [Hee+00, Seciton 4.9].

9. Introducing new projections

So far we have looked at three projections and assigned orientations to them. Apparently, three projections are not enough to reconstruct the object as well. In fact an infinite number of X-ray transforms is required to uniquely determine the density function f [Nat01, Theorem 3.5]. To introduce a new projection into a set of projections

with already known orientations we can compute the sinogram correlation functions of the new projection and already treated ones [Sch+95]. Although it is not necessary to determine all the common axes between all the projections, as the comparison with two projections would be enough, it is more likely that the projection will be correctly oriented with respect to the other already determined projections, if all of them are computed [FO92]. In [Hee+00] one can find a description of how the peaks of all the SCFs of all earlier projections with respect to the newly introduced projection can be used as an internal consistency check and help to eventually exclude poor projection images.

10. The Method of Common Lines in Practice

Raw projection images taken with an electron microscope are extremely noisy, meaning that they contain a large amount of extraneous information not related to the object. Thus they have a low *signal to noise ratio* (SNR), that is they have high noise relative to the signal given by the particle being observed. The common lines technique requires a high SNR in order to accurately find the common lines. The idea of how to increase the SNR is to find projections that have the same projection directions and put them together in a class of images. Then instead of using the individual projections, the average of all images in one class, a so called *class average*, is taken to determine the Euler angles. A good description of existing methods to increase the SNR can be found in [Hee+00, section 4.2-4.6] and [Fra06, chapters 3 and 4]. We will outline the steps that are typically taken prior to orientation reconstruction.

CTF-Correction and Filtering

After the individual particle images have been selected from the projection [Fra06, p.83], disturbing effects caused by the imaging conditions which are described by the *contrast transfer function* (CTF) are corrected, see [Fra06, p.53-64] and [Hee+00, p.317-323]. Moreover, in order to suppress disturbing frequencies a band-pass filter is applied to the particle images and unwanted background is removed by using a circular mask to the filtered images [Hee+00, section 4.1].

Alignment, Classification and Averaging

Before the images can be classified and averaged, they need to be aligned such that translational and rotational differences in the projection plane between the particles are

removed. Similar to the procedure for common line detection correlation functions are used. Again mutual correlation [HSO92] can be chosen over cross correlation in order to avoid bias towards dominant frequencies [Hee+00, section 4.2]. Another source of bias is the reference image that has to be chosen as a starting point of the alignment procedure. Reference free alignment techniques aim to avoid this issue [Hee+00, 4.3 and 4.4]. Both, reference-based and reference-free alignment procedures can be found in [Fra06, p.91-115].
After alignment of the particle images the categorization of similar particles into classes is carried out using one of several data analysis and image classification algorithms. A broad selection of techniques is described in [Fra06, p.176 ff.]. In the end all images in one class are averaged together what improves the SNR and is crucial for a correct assignment of the Euler angles.

11. Model Matching

The last section already raised the subject of enhancements used in practice, which are necessary due to the high amount of noise in the projections taken in cryo-EM. A commonly used tool to overcome this problem is iterative refinements, such as *model matching*. In a lot of cases some kind of initial model featuring structural properties of the particle is already known. This could be from other experiments such as cryo-electron tomography or the very popular random conical tilt method [Fra06, p. 210-212]. An example of model matching using the random conical tilt method can be found in [PGF94]. If this is not the case, it might be efficient to simply build a model using balls and sticks or, if one needs more precision, use the common line method to create a *'de novo'* model from scratch. In figure 11.1 the possible ways to obtain an initial model are depicted. Once such a model is available, reprojections are made and then compared to the experimental projections using cross-correlation. In this way it is possible to refine the before assigned Euler angles and realign and reclassify the projections. The refined class averages are then used to create a new model that usually has an improved resolution. The basic workflow is shown in figure 11.2. A disadvantage of this method can be that, if the initial model contains errors, the reprojections could have bias towards falsely assumed structures.

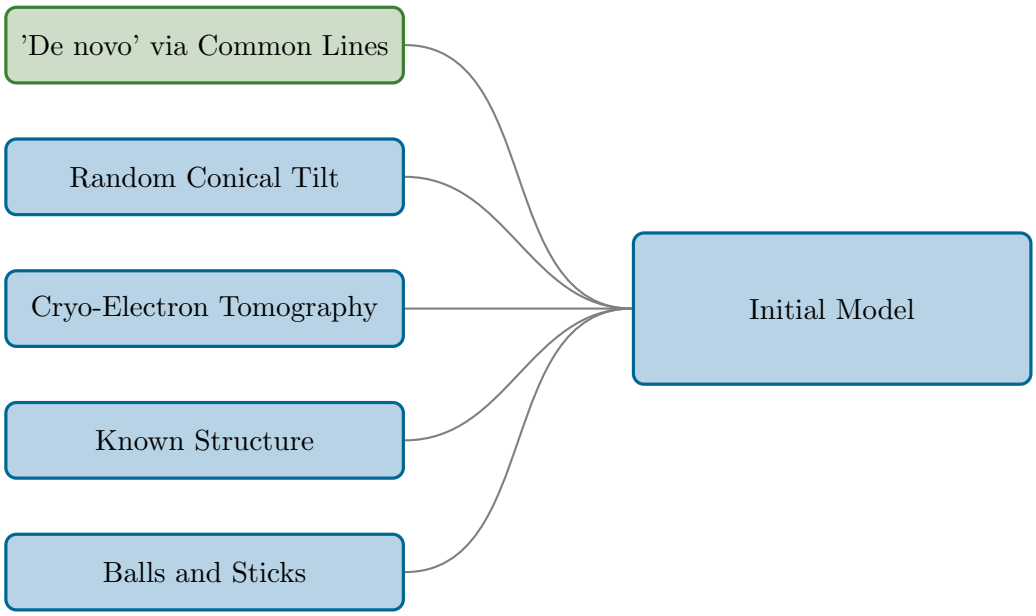

Figure 11.1.: Creating an initial model

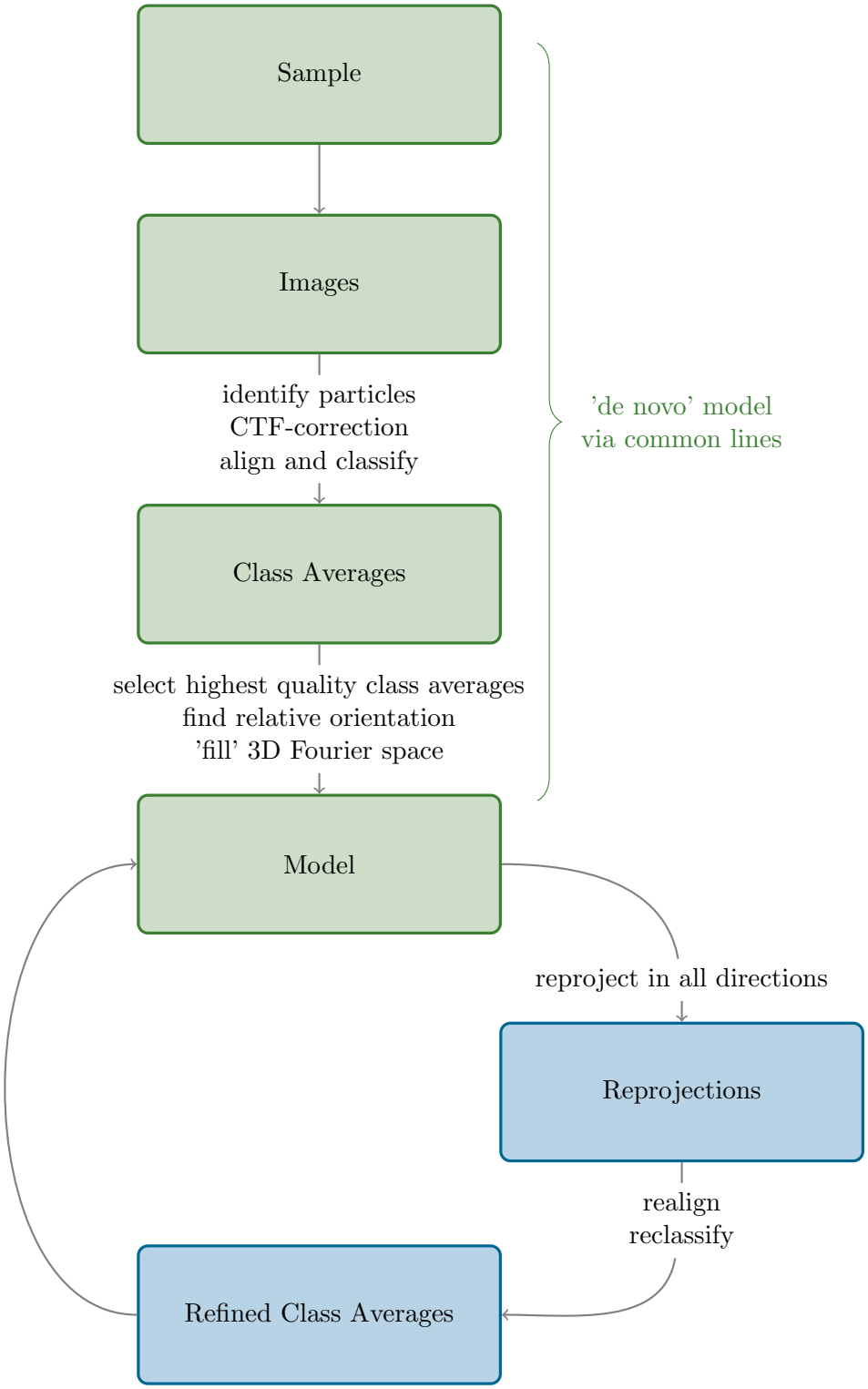

Figure 11.2.: Model Matching combined with Common Lines

IV. The moment method

The *moment method* was first introduced in [Gon88a] and [Gon88b], respectively. Unlike the method using *common lines* it is not restricted to three dimensions. The two-dimensional case is discussed in [BB00] and [LY07], we will only consider the problem in three dimensions. Moments in general are widely used in computer vision, pattern recognition, object identification, and object pose estimation, [MR98]. This chapter mainly follows [Lam08].

12. Geometric moments

As far as the problem of reconstructing projection orientations is concerned, we will work with *geometric moments* of a function, that is projections of that function onto monomials. They are the most simple amongst the moment functions.

Definition 12.1. *The* geometric moments *of a function* $f : \mathbb{R}^3 \to \mathbb{R}$ *are defined as*

$$m_{\boldsymbol{k}}(f) = \int_{\mathbb{R}^3} \boldsymbol{x}^{\boldsymbol{k}} f(\boldsymbol{x}) d\boldsymbol{x}$$

for some multiindex $\boldsymbol{k} = (k_1, k_2, k_3) \in \mathbb{N}^3$. *Note that* $\boldsymbol{x}^{\boldsymbol{k}} := x_1^{k_1} x_2^{k_2} x_3^{k_3}$. *The* order of the moment *is* $|\boldsymbol{k}| := k_1 + k_2 + k_3$.

Definition 12.2. *Let* $B = \{x \in \mathbb{R}^3 | \, \|x\| \leq 1\}$ *be the closed unit ball. For* $f \in L^1(B)$ *and* $K \in \mathbb{N}$ *we define the* moment vector *of* f, $\boldsymbol{m}_K(f)$, *as the vector consisting of all moments* $m_{\boldsymbol{k}}(f)$ *with* $|\boldsymbol{k}| \in K$. *By* $n(K)$ *we denote the dimension of this vector,* $\boldsymbol{m}_K(f) \in \mathbb{R}^{n(K)}$.

Note that usually the object's center of mass is put at the origin of the coordinate system. That means that the first order moments of the density function f are zero

$$\int_{\mathbb{R}^3} x_j f(\boldsymbol{x}) d\boldsymbol{x} = 0$$

for $j = 1, 2, 3$.
Remember that we denoted by $f_R(\boldsymbol{x}) = f(R\boldsymbol{x})$ the by $R = (\boldsymbol{R}^{(1)}, \boldsymbol{R}^{(2)}, \boldsymbol{R}^{(3)}) \in SO(3)$ transformed density. Making use of the *multinomial theorem* we can calculate its

moments

$$m_{\boldsymbol{k}}(f_R) = \sum_{\substack{|\boldsymbol{l}|=k_1\\|\boldsymbol{p}|=k_2\\|\boldsymbol{q}|=k_3}} \binom{k_1}{\boldsymbol{l}}\binom{k_2}{\boldsymbol{p}}\binom{k_3}{\boldsymbol{q}} m_{\boldsymbol{l}+\boldsymbol{p}+\boldsymbol{q}}(f)(\boldsymbol{R}^{(1)})^{\boldsymbol{l}}(\boldsymbol{R}^{(2)})^{\boldsymbol{p}}(\boldsymbol{R}^{(3)})^{\boldsymbol{q}}, \tag{12.1}$$

where

$$\binom{k_1}{\boldsymbol{l}} = \frac{k_1!}{l_1!l_2!l_3!}.$$

We get a polynomial equation of degree $|\boldsymbol{k}|$ in the entries of the rotation matrix. Moreover, we denote by $p_{(k_1,k_2)}(f,R)$ the moments of the projection of f at some orientation $R \in SO(3)$

$$p_{(k_1,k_2)}(f,R) = \int_{\mathbb{R}^2} x_1^{k_1} x_2^{k_2} \mathcal{P}(f,R) dx_1 dx_2. \tag{12.2}$$

By the definition of geometric moments the following analytic relation holds

$$p_{(k_1,k_2)}(f,R) = \int_{\mathbb{R}^2} x_1^{k_1} x_2^{k_2} \int_{\mathbb{R}} f(R\boldsymbol{x}) dx_3 dx_1 dx_2 = m_{(k_1,k_2,0)}(f_R). \tag{12.3}$$

From the data $\{\mathcal{P}(f,R_i), i \in I\}$ we can calculate the projection moments $p_{(k_1,k_2)}(f,R_i)$ for $(k_1,k_2) \in \mathbb{N}^2$ and $i \in I$. The *moment method* consists of solving for some finite set $K \subset \mathbb{N}$ the system

$$\sum_{\substack{|\boldsymbol{l}|=k_1\\|\boldsymbol{p}|=k_2}} \binom{k_1}{\boldsymbol{l}}\binom{k_2}{\boldsymbol{p}} m_{\boldsymbol{l}+\boldsymbol{p}}(f)(\boldsymbol{R}_i^{(1)})^{\boldsymbol{l}}(\boldsymbol{R}_i^{(2)})^{\boldsymbol{p}} = p_{(k_1,k_2)}(f,R_i). \tag{12.4}$$

The unknowns are the moments $m_{\boldsymbol{k}}(f)$ for $|\boldsymbol{k}| \in K$ and the orientations $R_i \in SO(3)$ for $i \in I$. Note that, if we find some solution $\boldsymbol{m}_K \in \mathbb{R}^{n(k)}$, we can always find some $f \in L^1(B)$ such that $\boldsymbol{m}_K(f) = \boldsymbol{m}_K$ by the following result [Lam08, Lemma 2.1.].

Lemma 12.3. *Let K be a finite subset of $\mathbb{N}$. Then $\{\boldsymbol{m}_K(f) | f \in L^1(B)\} = \mathbb{R}^{n(K)}$.*

Proof. The monomials $\boldsymbol{x}^{\boldsymbol{k}}$ defined as zero outside of B belong to $L^2(B)$. The moments of a function f can be written as the usual L^2 inner product $m_{\boldsymbol{k}}(f) = \langle \boldsymbol{x}^{\boldsymbol{k}}, f\rangle_{L^2}$. We now fix some $\tilde{\boldsymbol{k}}$ with $|\tilde{\boldsymbol{k}}| \in K$. It is sufficient to find an $f \in span\{\boldsymbol{x}^{\boldsymbol{k}}, |\boldsymbol{k}| \in K\} \subset L^2(B) \subset L^1(B)$, such that $\langle \boldsymbol{x}^{\tilde{\boldsymbol{k}}}, f\rangle_{L^2} \neq 0$ and $\langle \boldsymbol{x}^{\boldsymbol{k}}, f\rangle_{L^2} = 0$ for all other $\boldsymbol{k} \neq \tilde{\boldsymbol{k}}$ with $|\boldsymbol{k}| \in K$. Indeed, suppose $\langle \boldsymbol{x}^{\tilde{\boldsymbol{k}}}, f\rangle_{L^2} = 0$ for all $f \in \left(span\{\boldsymbol{x}^{\boldsymbol{k}}, |\boldsymbol{k}| \in K, \boldsymbol{k} \neq \tilde{\boldsymbol{k}}\}\right)^{\perp}$, where the orthogonal complement is taken within $span\{\boldsymbol{x}^{\boldsymbol{k}}, |\boldsymbol{k}| \in K\}$. Then $\boldsymbol{x}^{\tilde{\boldsymbol{k}}} \in$

$\left(\left(span\{\boldsymbol{x}^{\boldsymbol{k}}, |\boldsymbol{k}| \in K, \boldsymbol{k} \neq \tilde{\boldsymbol{k}}\}\right)^{\perp}\right)^{\perp} = span\{\boldsymbol{x}^{\boldsymbol{k}}, |\boldsymbol{k}| \in K, \boldsymbol{k} \neq \tilde{\boldsymbol{k}}\}$, which contradicts the assumption. □

Defining $\boldsymbol{R} = (R_i)_{i \in I}$, the vector consisting of the orientations R_i with $i \in I$, we can hence denote the unknowns shortly by $(\boldsymbol{m}_K(f), \boldsymbol{R}) \in \mathbb{R}^{n(K)} \times SO(3)^I$ or simply $(f, \boldsymbol{R}) \in L^1(B) \times SO(3)^I$. The question that arises is what assumptions on K, the number of projections and an object have to be made in order to find a unique solution to the problem. The most challenging part will be to characterize the class of objects.

13. Uniqueness up to an Orthogonal Transformation

We already know from the method of common lines that the absolute orientation of the projection orientations and the handedness of the system can be chosen arbitrarily. Hence, solutions to (12.4) are unique only up to an orthogonal transformation. Let $(f, \boldsymbol{R}) \in L^1(B) \times SO(3)^I$ be a solution of (12.4). Then for all $U \in O(3)$ and $R \in SO(3)$ we have

$$m_{\boldsymbol{k}}(f_R) = m_{\boldsymbol{k}}((f_U)_{U^T R}).$$

Thus, also $(f_U, \hat{\boldsymbol{R}}) \in L^1(B) \times SO(3)^I$ is a solution, where

$$\hat{R}_i = \begin{cases} U^T R_i, & \text{if } det(U) = 1, \\ U^T R_i \Sigma, & \text{if } det(U) = -1, \end{cases} \tag{13.1}$$

for all $i \in I$ and

$$\Sigma = \begin{pmatrix} 1 & 0 & 0 \\ 0 & 1 & 0 \\ 0 & 0 & -1 \end{pmatrix} \in O(3) \tag{13.2}$$

is a reflection. We define the following equivalence relation.

Definition 13.1. *Let $f, g \in L^1(B)$, $K \in \mathbb{N}$ and $\boldsymbol{R} = (R_i)_{i \in I}, \hat{\boldsymbol{R}} = (\hat{R}_i)_{i \in I}$ be orientation vectors. Then*

$$(\boldsymbol{m}_K(f), \boldsymbol{R}) \sim (\boldsymbol{m}_K(g), \hat{\boldsymbol{R}}), \tag{13.3}$$

if there exists $U \in O(3)$ such that $\boldsymbol{m}_K(g) = \boldsymbol{m}_K(f_U)$ and $\hat{R}_i = U^T R_i$ for all $i \in I$ or $\hat{R}_i = U^T R_i \Sigma$ for all $i \in I$.

14. Conditions for the Object f

We now want to find out what the density function f needs to fulfill in order to obtain a unique solution of system (12.4). This is strongly connected to the method of common lines. There, one of our assumptions has been that for two different projection orientations R_i and R_j we get two different corresponding projection images P_i and P_j, so that the object of interest is asymmetric, or at least, in the case of symmetric particles, that we know the symmetric structures and find a range of projection directions in which the assumption holds. In further consequence this leads to the situation of the two projections having exactly one common line. Lamberg somehow uses the same idea in [Lam08] in a more abstract way and with tools from algebraic geometry to shows that there is a certain generic set of objects for which the method gives unique results.

For the sake of simplicity we go back to definition 3.4 of the X-ray transform using viewing directions, that are the third columns of the projections orientations, instead of rotation matrices.

Following the original notation we get for $\boldsymbol{\omega} \in S^2$ the fundamental relation between the *X-ray* and the *Radon transform* [Nat01, Chapter II, equation (1.1)],

$$\mathcal{R}f(\boldsymbol{\omega}, s) = \int\limits_{\substack{\boldsymbol{x}\in\boldsymbol{\theta}^\perp \\ \boldsymbol{x}\cdot\boldsymbol{\omega}=s}} \mathcal{P}f(\boldsymbol{\theta}, \boldsymbol{x})d\boldsymbol{x}, \tag{14.1}$$

for any $\boldsymbol{\theta} \in S^2$ with $\boldsymbol{\theta} \perp \boldsymbol{\omega}$.

Consequently instead of first taking the X-ray transform along a line in some direction $\boldsymbol{\theta}$, obtaining a two-dimensional projection, and doing that again by taking the Radon transform of that two-dimensional projection in the direction of $\boldsymbol{\omega}$, we can combine those two steps and directly integrate along the planes $\boldsymbol{\omega} \cdot \boldsymbol{x} = s$.

To illustrate the connection to the common lines let us consider such an integral along the plane $\boldsymbol{\omega}_1 \cdot \boldsymbol{x} = s$. According to 14.1 we can find two directions $\boldsymbol{\theta}_1, \boldsymbol{\theta}_2 \in S^2$ with $\boldsymbol{\theta}_1 \perp \boldsymbol{\omega}_1$ and $\boldsymbol{\theta}_2 \perp \boldsymbol{\omega}_1$ such that the Radon transforms with respect to $\boldsymbol{\omega}_1$ of projections in those directions have the same values.

$$\mathcal{R}f(\boldsymbol{\omega_1}, s) = \int\limits_{\substack{\boldsymbol{x}\in\boldsymbol{\theta}_1^\perp \\ \boldsymbol{x}\cdot\boldsymbol{\omega}_1=s}} \mathcal{P}f(\boldsymbol{\theta_1}, \boldsymbol{x})d\boldsymbol{x} = \int\limits_{\substack{\boldsymbol{x}\in\boldsymbol{\theta}_2^\perp \\ \boldsymbol{x}\cdot\boldsymbol{\omega}_1=s}} \mathcal{P}f(\boldsymbol{\theta_2}, \boldsymbol{x})d\boldsymbol{x}$$

With the restrictions $\boldsymbol{x} \in \boldsymbol{\theta}_1^\perp$ and $\boldsymbol{x} \in \boldsymbol{\theta}_2^\perp$ for the vectors $\boldsymbol{x} \in \mathbb{R}^3$ the integrals over $\boldsymbol{x} \cdot \boldsymbol{\omega}_1 = s$ are just line integrals in $\boldsymbol{\theta}_1^\perp$ and $\boldsymbol{\theta}_2^\perp$ in certain directions dependent on $\boldsymbol{\omega}_1$. These directions are exactly the ones defining the common line between $\mathcal{P}f(\boldsymbol{\theta_1}, \cdot)$ and $\mathcal{P}f(\boldsymbol{\theta_2}, \cdot)$. Hence, a pair of angles defining the common line between two projections corresponds to the integral along a certain plane. In the method of common lines it is crucial to find for two different projections exactly one common line. In terms of the Radon transform we can formulate the following assumption.

Assumption 1. *Let $f \in L^1(B)$ be such that if the Radon transform of f coincides at directions $\boldsymbol{\omega}_1 \in S^2$ and $\boldsymbol{\omega}_2 \in S^2$,*

$$\mathcal{R}f(\boldsymbol{\omega_1}, s) = \mathcal{R}f(\boldsymbol{\omega_2}, s) \tag{14.2}$$

for all $s \in \mathbb{R}$, then $\boldsymbol{\omega}_1 = \boldsymbol{\omega}_2$.

14.1. Helgason-Ludwig consistency conditions

Indeed, the range of the Radon transform is highly structured. Not any function is the Radon transform of another function, as it holds that the geometric moments of the Radon transform must be homogeneous polynomials, that is polynomials whose nonzero terms all have the same degree, of a certain form. In applications where the data is assumed to be the Radon transform of some unknown function, one can use that correspondence to check whether the data is consistent in the sense of that property. These conditions are therefore called *Helgason-Ludwig consistency conditions* and can for example be found in [Nat01, Theorem 4.1 and Theorem 4.2] or [Hel99, Lemma 2.3.].

Theorem 14.1 (Helgason-Ludwig consistency conditions)**.** *Let $f \in \mathcal{S}(\mathbb{R}^3)$. For $n \in \mathbb{N}_0$ it holds that*

$$\int_{\mathbb{R}} s^n \mathcal{R}f(\boldsymbol{\omega}, s) ds = \int_{\mathbb{R}^3} (\boldsymbol{x} \cdot \boldsymbol{\theta})^n f(\boldsymbol{x}) d\boldsymbol{x}. \tag{14.3}$$

When first introducing the method of moments Goncharov [Gon88a] used this consistency conditions to associate to the object f an ellipsoid described by

$$\int_{\mathbb{R}^3} (\boldsymbol{x} \cdot \boldsymbol{\theta})^2 f(\boldsymbol{x}) d\boldsymbol{x} = 1,$$

as can be seen in [Gon88a; Gon90]. If the lengths of the main axes of this ellipsoid corresponding to f are pairwise distinct, any transform R which is not the identity transforms it into an ellipsoid different from the first one. The main idea of the

method is now to look at the ellipsoid corresponding to the transformed object f_R. The transformation R is then uniquely determined by comparing them. It is assumed that for an asymmetric object f the main axes are pairwise distinct.
Hence, in contrast to assumption 1 Goncharov compares the second order moments of the Radon transforms rather than the Radon transforms themselves. Lamberg [Lam08] adapted that idea and generalized it in view of the order of moments. Using again the multinomial theorem it holds that

$$Q_n(f,\boldsymbol{\omega}) := \int_{\mathbb{R}^3} (\boldsymbol{x}\cdot\boldsymbol{\omega})^n f(\boldsymbol{x})d\boldsymbol{x} = \sum_{|\boldsymbol{k}|=n} \binom{n}{\boldsymbol{k}} m_{\boldsymbol{k}}(f)\boldsymbol{\omega}^{\boldsymbol{k}}.$$

Keeping in mind the idea from before, we assume for the object f the following.

Assumption 2. *Let $f \in L^1(B)$ be such that if the moments of 'certain orders' $n \in \mathbb{N}$ of the Radon transform of f coincide at directions $\boldsymbol{\omega}_1 \in S^2$ and $\boldsymbol{\omega}_2 \in S^2$,*

$$Q_n(f,\boldsymbol{\omega}_1) = Q_n(f,\boldsymbol{\omega}_2), \tag{14.4}$$

then $\boldsymbol{\omega}_1 = \boldsymbol{\omega}_2$.

It is not clear so far which orders of the moments should be compared. The infinite set of all moments exactly determines the object f [Tea80], what would bring us back to assumption 1. In his paper Lamberg uses tools from algebraic geometry to study for $\boldsymbol{x},\boldsymbol{y} \in \mathbb{C}^3$ and $H = \{2,3,5,7,d\}, d \in \mathbb{N}^+ \setminus \{2,3,5,7\}$ the more abstract system of equations

$$\begin{aligned} \sum_{j=1}^{3} x_i^2 - \sum_{j=1}^{3} y_i^2 &= 0, \\ \sum_{|\boldsymbol{k}|=n} \binom{n}{\boldsymbol{k}} m_{\boldsymbol{k}} \boldsymbol{x}^{\boldsymbol{k}} - \sum_{|\boldsymbol{k}|=n} \binom{n}{\boldsymbol{k}} m_{\boldsymbol{k}} \boldsymbol{y}^{\boldsymbol{k}} &= 0, \end{aligned} \tag{14.5}$$

with unknowns $(\boldsymbol{m}_H, \boldsymbol{x}, \boldsymbol{y}) \in \mathbb{C}^{n(H)} \times \mathbb{C}^6$. In the light of assumption 2 we consider $\boldsymbol{x},\boldsymbol{y} \in S^2$. Then the point $(\boldsymbol{m}_H(f), \boldsymbol{x}, \boldsymbol{y}) \in \mathbb{R}^{n(H)} \times \mathbb{R}^6$ is a solution to (14.5), if and only if

$$Q_n(f,\boldsymbol{x}) = Q_n(f,\boldsymbol{y}) \text{ for all } n \in H. \tag{14.6}$$

The choice of the set H might seem a bit odd, but will turn out to be the optimal one regarding the set of desirable objects f.
Let now $\mathcal{M}_H \in \mathbb{R}^{n(H)}$ be the set of coefficient vectors $\boldsymbol{m}_H \in \mathbb{R}^{n(H)}$, for which system

(14.5) has only the trivial solutions $(\boldsymbol{x}, \boldsymbol{x}), \boldsymbol{x} \in \mathbb{C}^3$ and let $\mathcal{A}_H = \mathbb{R}^{n(H)} \setminus \mathcal{M}_H$. Our final assumption for the density function f will then be the following.

Assumption 3. *Let $f \in L^1(B)$ define a vector $\boldsymbol{m}_H$ for which system (14.5) has only the trivial solutions $(\boldsymbol{x}, \boldsymbol{x})$, that is let*

$$f \in \mathcal{O}_H := \{f \in L^1(B) \mid \boldsymbol{m}_H(f) \in \mathcal{M}_H\}.$$

To describe the size of $\mathcal{O}_H$ we need to define the following.

Definition 14.2. *A subset of a topological space X is* nowhere dense, *if its closure has empty interior. We say that a set is* generic *in X, if its complement is* nowhere dense *in X.*

Lamberg proves in [Lam08, Section3] that the set $\mathcal{O}_H$ is generic in the space $L^1(B)$.

Theorem 14.3. *For $H = \{2, 3, 5, 7, d\}, d \in \mathbb{N}_+ \setminus \{2, 3, 5, 7\}$, the set $\mathcal{A}_H$ is nowhere dense and of Lebesgue measure zero in $\mathbb{R}^{n(H)}$.*

From this we get the subsequent corollary [Lam08, Corollary 1].

Corollary 14.4. *For $H = \{2, 3, 5, 7, d\}, d \in \mathbb{N}_+ \setminus \{2, 3, 5, 7\}$ the set $\mathcal{O}_H$ is generic in $L^1(B)$.*

15. Uniqueness results

Having found a set of density functions f and restricted the order of the considered moments accordingly, we can go back to system 12.4 and discuss the uniqueness results for the moment method given in [Lam08]. By its own nature in this method not only the projection orientations are recovered, but using the same equation also the object itself. So let $(f, R_i)_{i \in I}$ and $(g, \hat{R}_i)_{i \in I} \in L^1(B) \times SO(3)$ be solutions of (12.4), then they satisfy

$$m_{(k_1,k_2,0)}(f_{R_i}) = m_{(k_1,k_2,0)}(g_{\hat{R}_i})$$

for all $k_1 + k_2 \in K \subset \mathbb{N}$ and $i \in I$. The first theorem restates what we already know from the common line method, namely that we need three different projections in order to reconstruct the projection orientations.

Theorem 15.1. *Let $H = \{2, 3, 5, 7, d\}, d \in \mathbb{N}_+ \setminus \{2, 3, 5, 7\}, f, g \in L^1(B)$ and let $\boldsymbol{R} = (R_i)_{i \in I}$ and $\hat{\boldsymbol{R}} = (\hat{R}_i)_{i \in I}$ be orientation vectors.*

Suppose $f \in \mathcal{O}_H$ *and* $\{\boldsymbol{R}_i^{(3)} \mid i \in I\}$ *contains three linearly independent projection directions. If*

$$m_{(k_1,k_2,0)}(f_{R_i}) = m_{(k_1,k_2,0)}(g_{\hat{R}_i})$$

for all $k_1 + k_2 \in H$ *and* $i \in I$*, there exists an orthogonal matrix* $U \in O(3)$ *such that*

$$\hat{R}_i = U^T R_i \text{ for all } i \in I$$

or

$$\hat{R}_i = U^T R_i \Sigma \text{ for all } i \in I,$$

where Σ *has been defined in 13.2.*

The proof is based exactly on the constructive method of common lines.
In the moment method not only the projection directions are recovered, but from the same system also some of the moments of the function f can be found as part of the solution. The next theorem states that given $k+1$ projections the moments of orders up to k are uniquely recovered.

Theorem 15.2. *Let* $H = \{2,3,5,7,d\} \subset K \subset \mathbb{N}, d \in \mathbb{N}_+ \setminus \{2,3,5,7\}$*, where* K *is arbitrary. Moreover let* $f, g \in L^1(B)$ *and let* $\boldsymbol{R} = (R_i)_{i\in I}$ *and* $\hat{\boldsymbol{R}} = (\hat{R}_i)_{i\in I}$ *be orientation vectors.*
Suppose $f \in \mathcal{O}_H$ *and* $\{\boldsymbol{R}_i^{(3)} \mid i \in I\}$ *satisfies the following conditions:*

(i) It contains three linearly independent projection directions.

(ii) The number of projection directions modulo π *is greater or equal to* $\sup_{k\in K} k+1$*.*

If

$$m_{(k_1,k_2,0)}(f_{R_i}) = m_{(k_1,k_2,0)}(g_{\hat{R}_i})$$

for all $k_1 + k_2 \in H$ *and* $i \in I$*, then*

$$(\boldsymbol{m}_K(f), \boldsymbol{R}) \sim (\boldsymbol{m}_K(g), \hat{\boldsymbol{R}}).$$

For a proof see [Lam08, section 4]. The last theorem is concerned with the unique recovery of the density function itself. Though not available in practice, in general an infinite number of projections is needed to recover the object [Nat01, Theorem 3.5].

Theorem 15.3. *Let* $H = \{2,3,5,7,d\}, d \in \mathbb{N}_+ \setminus \{2,3,5,7\}, f, g \in L^1(B)$*. Let* $\boldsymbol{R} = (R_i)_{i\in I}$ *and* $\hat{\boldsymbol{R}} = (\hat{R}_i)_{i\in I}$ *be orientation vectors, where the index set* I *is infinite.*
Suppose $f \in \mathcal{O}_H$ *and* $\{\boldsymbol{R}_i^{(3)} \mid i \in I\}$ *satisfies the following conditions*

(i) It contains a linearly independent triplet.

(ii) The number of projection directions is infinite.

If the projections coincide

$$P(f, R_i) = P(g, \hat{R}_i)$$

for all $i \in I$, there exists an orthogonal matrix $U \in O(3)$ such that

$$f_U = g.$$

Proof. The assumptions of theorem 15.2 are satisfied for $K = \mathbb{N}$ and we can find a $U \in SO(3)$ such that $m_{\boldsymbol{k}}(g) = m_{\boldsymbol{k}}(f_U)$ for all $\boldsymbol{k} \in \mathbb{N}^3$. That is

$$\int_{\mathbb{R}^3} \boldsymbol{x}^{\boldsymbol{k}}(g(\boldsymbol{x}) - f_U(\boldsymbol{x}))d\boldsymbol{x} = 0.$$

The polynomials are dense in the space of continuous real functions by the *Stone-Weierstrass theorem*. Thus it also holds for all $\phi : \mathbb{R}^3 \to \mathbb{R}$ with $\phi \in C(B)$ that

$$\int_{\mathbb{R}^3} \phi(\boldsymbol{x})(g(\boldsymbol{x}) - f_U(\boldsymbol{x}))d\boldsymbol{x} = 0.$$

The fundamental lemma of calculus of variations, see for example [Gia04, Lemma 3,p.32], gives $f_U = g$ in $L^1(B)$. □

V.Appendix

Abstract

In the field of structural biology cryo-electron microscopy, or cryo-EM for short, is a nowadays popular method for studying the architecture of macromolecules. One subdiscipline of this technique which is particularly interesting from a mathematical point of view is single particle cryo-electron microscopy. Other inverse problems appearing in imaging are concerned with the reconstruction of an object from a set of projections in given directions. In the case of single particle cryo-EM, not only the object itself is unknown, but also the directions from which the projections are taken are completely random. In this thesis different methods for reconstructing the projection directions are presented with particular focus on uniqueness results. Moreover, it aims at giving an overview of some techniques used in practice.

Zusammenfassung

Kryo-Elektronenmikroskopie, oder kurz Kryo-EM, ist im Gebiet der Strukturbiologie ein wichtiges Werkzeug um den Aufbau von Makromolekülen zu untersuchen. Ein in mathematischer Hinsicht interessantes Problem taucht auf, wenn man Kryo-EM in Kombination mit Einzelpartikelanalyse betrachtet. Andere inverse Probleme aus dem Feld der bildgebenden Verfahren bestehen in erster Linie darin ein Objekt anhand vieler Projektionen in gewissen Richtungen zu rekonstruieren. Im Falle von Einzelpartikel-Kryo-Elektronenmikroskopie ist nicht nur das Objekt selbst unbekannt, sondern auch die Projektionsrichtungen zufällig. In dieser Arbeit beschäftigen wir uns mit verschiedenen Methoden, um diese unbekannten Projektionsrichtungen zu rekonstruieren, wobei wir insbesondere Wert auf die Frage der Eindeutigkeit dieser Rekonstruktion legen. Außerdem wird ein Überblick über unterschiedliche Techniken, die in der Praxis verwendet werden, gegeben.

Danksagung

An dieser Stelle möchte ich mich bei all jenen bedanken, die mich während der Anfertigung dieser Masterarbeit unterstützt und motiviert haben.

Zuerst möchte ich mich bei Otmar Scherzer bedanken, der meine Masterarbeit betreut und begutachtet hat. Seine Anregungen und kritischen Fragen haben mir sehr weitergeholfen und mich stets dazu angespornt meine Arbeit noch weiter zu verbessern. Insbesondere hat er es mir ermöglicht an einem eigenen Schreibtisch zu arbeiten und hat für eine äußerst angenehme Arbeitumgebung gesorgt (Couch). Danke dafür.

Mein Dank gilt auch allen Mitgliedern des Computational Science Centers, die mich von Anfang an in die Arbeitsgruppe integriert haben und deren Bürotüren bei Fragen immer für mich offen standen. Insbesondere möchte ich mich bei meinen Bürokolleginnen Cong und Melanie für die tolle Stimmung und ihre motivierenden Worte bedanken. Außerdem bedanke ich mich bei Peter, der sich jederzeit für fachliche und private Plaudereien Zeit genommen hat und mir vor allem beim Erstellen der Bilder sehr geholfen hat.

Meinen Freunden und meiner Familie danke ich für ihre unermüdliche Unterstützung und für den starken emotionalen Rückhalt über die Dauer meines gesamten Studiums. Besonderer Dank gilt Jan, der immer für mich da war und an mich geglaubt hat. Außerdem danke ich Basti, ohne den diese Arbeit nicht möglich gewesen wäre.

Bibliography

[BB00] S. Basu and Y. Bresler. "Uniqueness of tomography with unknown view angles". In: *IEEE Trans. Image Process.* 9.6 (June 2000), pp. 1094–1106. ISSN: 1057-7149. DOI: 10.1109/83.846251.

[Bra78] R. N. Bracewell. *The Fourier Transform and its Applications*. New York: McGraw-Hill, 1978.

[CDK70] R. A. Crowther, D. J. DeRosier and A. Klug. "The Reconstruction of a Three-Dimensional Structure from Projections and its Application to Electron Microscopy". In: *Proc. Roy. Soc. Lond. A.* 317.1530 (1970), pp. 319–340. ISSN: 0080-4630. DOI: 10.1098/rspa.1970.0119. URL: http://rspa.royalsocietypublishing.org/content/317/1530/319.

[Che15] Y. Cheng. "Single-particle cryo-EM at crystallographic resolution". In: *Cell* 161.3 (2015), pp. 450–457. ISSN: 0092-8674. DOI: 10.1016/j.cell.2015.03.049.

[Cro71] R.A. Crowther. "Procedures for Three-Dimensional Reconstruction of Spherical Viruses by Fourier Synthesis from Electron Micrographs". In: *Philos. Trans. Roy. Soc. Lond.* 261.837 (1971), pp. 221–228. ISSN: 00804622. URL: http://www.jstor.org/stable/2417109.

[Doa+03] D.N.P. Doan et al. "Three-dimensional reconstruction of hibiscus chlorotic ringspot virus". In: *J. Struct. Biol.* 144.3 (2003), pp. 253–261. ISSN: 1047-8477.

[FO92] N.A. Farrow and F.P. Ottensmeyer. "A posteriori determination of relative projection directions of arbitrarily oriented macromolecules". In: *J. Opt. Soc. Amer. A* 9 (1992), pp. 1749–1760. DOI: 10.1364/JOSAA.9.001749.

[Fra06] J. Frank. *Three-Dimensional Electron Microscopy of Macromolecular Assemblies: Visualization of Biological Molecules in Their Native State*. Oxford University Press, 2006. ISBN: 9780198034384. URL: https://books.google.at/books?id=kjGKy2LeWnUC.

[Gia04] S. Giaquinta M. Hildebrandt. *Calculus of Variations I*. Vol. 310. Grundlehren der mathematischen Wissenschaften. Springer Berlin Heidelberg, 2004. DOI: 10.1007/978-3-662-03278-7.

[Gon88a] A. B. Goncharov. "Integral geometry and three-dimensional reconstruction of randomly oriented identical particles from their electron microphotos". In: *Acta Appl. Math.* 11.3 (1988), pp. 199–211. DOI: 10.1007/BF00140118. URL: http://dx.doi.org/10.1007/BF00140118.

[Gon88b] A. B. Goncharov. "Methods of integral geometry and recovering a function with compact support from its projections in unknown directions". In: *Acta Appl. Math.* 11.3 (1988), pp. 213–222. DOI: 10.1007/BF00140119. URL: http://dx.doi.org/10.1007/BF00140119.

[Gon90] A.B. Goncharov. "Three-Dimensional Reconstruction of Arbitrarily Arranged Identical Particles Given their Projections". In: *Mathematical Problems of Tomography*. Ed. by I.M. Gelfand and S.G. Gindikin. Translations of Mathematical Monographs 81. Providence, Rhode Island: American Mathematical Society, 1990, pp. 67–95. ISBN: 0-8218-4534-9.

[Hee+00] M. van Heel et al. "Single-particle electron cryo-microscopy: towards atomic resolution". In: *Quart. Rev. Biophys.* 33.4 (2000), pp. 307–369. DOI: 10.1017/s0033583500003644.

[Hee+97] M. van Heel et al. "Angular reconstitution in three-dimensional electron microscopy: historical and theoretical aspects". In: *Scan. Mic.* (1997), pp. 195–210.

[Hee87] M. van Heel. "Angular reconstitution: A posteriori assignment of projection directions for 3D reconstruction". In: *Ultramicr.* 21.2 (1987), pp. 111–123. ISSN: 0304-3991. DOI: 10.1016/0304-3991(87)90078-7. URL: http://www.sciencedirect.com/science/article/pii/0304399187900787.

[Hel99] S. Helgason. *The Radon transform*. 2nd ed. Vol. 5. Progress in Mathematics. Boston, MA: Birkhäuser Boston Inc., 1999. xiv+188. ISBN: 0-8176-4109-2.

[HS11] R. Hadani and A. Singer. "Representation theoretic patterns in three dimensional Cryo-Electron Microscopy I: The intrinsic reconstitution algorithm". In: *Ann. Math.* 174.2 (2011), pp. 1219–1241. ISSN: 0003486X. URL: http://www.jstor.org/stable/23030523.

[HSO92] M. van Heel, M. Schatz and E. Orlova. "Correlation functions revisited". In: *Ultramicr.* 46.1 (1992), pp. 307–316. ISSN: 0304-3991. DOI: 10.1016/0304-3991(92)90021-B. URL: http://www.sciencedirect.com/science/article/pii/030439919290021B.

[Lam08] L. Lamberg. "Unique recovery of unknown projection orientations in three-dimensional tomography". In: *Inverse Probl. Imaging* 2.4 (2008), pp. 547–575. DOI: 10.3934/ipi.2008.2.547. URL: http://dx.doi.org/10.3934/ipi.2008.2.547.

[LY07] L. Lamberg and L. Ylinen. "Two-dimensional tomography with unknown view angles". In: *Inverse Probl. Imaging* 1.4 (2007), pp. 623–642. DOI: 10.3934/ipi.2007.1.623. URL: http://dx.doi.org/10.3934/ipi.2007.1.623.

[Mal+06] S. P. Mallick et al. "Structure and View Estimation for Tomographic Reconstruction: A Bayesian Approach". In: *2006 IEEE Computer Society Conference on Computer Vision and Pattern Recognition (CVPR'06)*. Vol. 2. 2006, pp. 2253–2260. DOI: 10.1109/CVPR.2006.295.

[MB73] B.W. Matthews and S.A. Bernhard. "Structure and symmetry of oligomeric enzymes". In: *Annu. Rev. Biomed. Eng.* 2 (1973), pp. 257–317. DOI: 10.1146/annurev.bb.02.060173.001353.

[Mil+13] J.L.S. Milne et al. "Cryo-electron microscopy – a primer for the non-microscopist". In: *FEBS Journal* 280.1 (2013), pp. 28–45. ISSN: 1742-4658. DOI: 10.1111/febs.12078. URL: http://dx.doi.org/10.1111/febs.12078.

[MR98] R. Mukundan and K.R. Ramakrishnan. *Moment Functions in Image Analysis: Theory and Applications*. World Scientific, 1998. ISBN: 9789810235246.

[Nat01] F. Natterer. *The mathematics of computerized tomography*. Vol. 32. Classics in Applied Mathematics. Reprint of the 1986 original. Philadelphia, PA: Society for Industrial and Applied Mathematics (SIAM), 2001. xviii+222. ISBN: 0-89871-493-1.

[PGF94] P.A. Penczek, R.A. Grassucci and J. Frank. "The ribosome at improved resolution: New techniques for merging and orientation refinement in 3D cryo-electron microscopy of biological particles". In: *Ultramicr.* 53.3 (1994), pp. 251–270. ISSN: 0304-3991. DOI: http://dx.doi.org/10.1016/0304-3991(94)90038-8. URL: http://www.sciencedirect.com/science/article/pii/0304399194900388.

[PZF96] P.A. Penczek, J. Zhu and J. Frank. "A common-lines based method for determining orientations for N ¿ 3 particle projections simultaneously". In: *Ultramicr.* 63.3 (1996), pp. 205–218. ISSN: 0304-3991. DOI: 10.1016/0304-

3991(96)00037-X. URL: http://www.sciencedirect.com/science/article/pii/030439919600037X.

[Sch+95] M. Schatz et al. "Structure of Lumbricus terrestris Hemoglobin at 30 Å Resolution Determined Using Angular Reconstitution". In: *Journal of Structural Biology* 114.1 (1995), pp. 1047–8477. DOI: http://dx.doi.org/10.1006/jsbi.1995.1003. URL: http://www.sciencedirect.com/science/article/pii/S1047847785710039.

[Sch+97] M. Schatz et al. "Angular reconstruction in three-dimensional electron microscopy: Practical and technical aspects". In: *Scanning Microscopy* 33.4 (1997), pp. 197–193.

[Sin+10] A. Singer et al. "Detecting Consistent Common Lines in Cryo-EM by Voting". In: *Journal of Structural Biology* 169 3 (2010), pp. 312–22.

[SS11] A. Singer and Y. Shkolnisky. "Three-dimensional Structure Determination from Common Lines in Cryo-EM by Eigenvectors and Semidefinite Programming". In: *SIAM J. Imaging Sciences* 4.2 (2011), pp. 543–572. DOI: 10.1137/090767777. URL: http://dx.doi.org/10.1137/090767777.

[SS12] A. Singer and Y. Shkolnisky. "Viewing Direction Estimation in Cryo-EM Using Synchronization". In: *SIAM J. Imaging Sciences* 5.3 (2012), pp. 1088–1110. DOI: 10.1137/120863642. URL: http://dx.doi.org/10.1137/120863642.

[Tea80] M.R. Teague. "Image analysis via the general theory of moments". In: *Journal of the Optical Society of America* 70.8 (Aug. 1980), pp. 920–930. DOI: 10.1364/JOSA.70.000920. URL: http://www.osapublishing.org/abstract.cfm?URI=josa-70-8-920.

[WSW13] L. Wang, A. Singer and Z. Wen. "Orientation determination of cryo-EM images using least unsquared deviations". In: *SIAM J. Imaging Sciences* 6.4 (2013), pp. 2450–2483. DOI: 10.1137/130916436. URL: http://dx.doi.org/10.1137/130916436.

[Zho08] Z.H. Zhou. "Towards atomic resolution structural determination by single-particle cryo-electron microscopy". In: *Curr. Opin. Struct. Biol.* 18.2 (2008), pp. 218–228. ISSN: 0959-440X. DOI: 10.1016/j.sbi.2008.03.004. URL: http://www.sciencedirect.com/science/article/pii/S0959440X08000365.